Permian–Middle Triassic floral succession in North China and implications for the great transition of continental ecosystems

Shu, Wenchao; Tong, Jinan; Yu, Jianxin; Hilton, Jason; Benton, Michael J.; Shi, Xiao; Diez, Jose; Wignall, Paul; Chu, Daoliang; Tian, Li; Yi, Zhixing; Yao, Yongdong

DOI:
10.1130/B36316.1

Permian–Middle Triassic floral succession in North China and implications for the great transition of continental ecosystems

Wenchao Shu[1], Jinnan Tong[1,*], Jianxin Yu[1,*], Jason Hilton[2], Michael J. Benton[3], Xiao Shi[4], José B. Diez[5], Paul B. Wignall[6], Daoliang Chu[1], Li Tian[1], Zhixing Yi[1], and Yongdong Mao[7]

[1]*State Key Laboratory of Biogeology and Environmental Geology, School of Earth Sciences, China University of Geosciences, Wuhan 430074, China*

[2]*School of Geography, Earth and Environmental Sciences and Birmingham, Institute of Forest Research, The University of Birmingham, Edgbaston, Birmingham B15 2TT, UK*

[3]*School of Earth Sciences, Life Sciences Building, University of Bristol, Bristol, BS8 1TQ, UK*

[4]*School of Earth Sciences, Jilin University, Changchun 130061, China*

[5]*Departamento de Xeociencias Mariñas e Ordenación do Territorio, Facultade de Ciencias do Mar, Universidade de Vigo, Vigo 36310, Spain*

[6]*School of Earth and Environment, University of Leeds, Leeds LS2 9JT, UK*

[7]*Shanxi Institute of Geological Survey, Taiyuan 030006, China*

*Corresponding author. Emails: jntong@cug.edu.cn; yujianxin@cug.edu.cn.

ABSTRACT

The global pattern of plant evolution through the Permian–Triassic mass extinction is uncertain, and the extent to which land plants were affected is debated. Detailed studies undertaken at a regional scale can help evaluate this floral transition, and thus

we provide a detailed account of floral evolution from the Permian to Middle Triassic of North China based on new paleobotanical data and a refined biostratigraphy. Five floral transition events are identified from before, during and after the Permian–Triassic crisis, including the disappearance of the gigantopterid flora (associated with loss of coal deposits), the end-Permian mass extinction of Paleophytic taxa, and gradual recovery in the Triassic with stepwise appearance of the Mesophytic vegetation. The record begins with a Cisuralian gigantopterid-dominated rainforest community, and then a Lopingian walchian Voltziales conifer–ginkgophyte community that evolved into a voltzialean conifer-pteridosperm forest community. The last is associated with a change amongst terrestrial vertebrates from the Jiyuan fauna to a pareiasaur-dominated fauna, found in red beds that lack coal deposits due to arid conditions. The disappearance of the voltzialean conifer forest community may represents the end-Permian mass extinction of plants although it could also be a consequence of the non-preservation of plants in sedimentary red-beds. The first post-crisis plants are an Induan herbaceous lycopsid community, succeeded by the *Pleuromeia-Neocalamites* shrub marsh community. A pteridosperm shrub woodland community dominated for a short time in the late Early Triassic along with the reappearance of insect herbivory. Finally, in the Middle Triassic, gymnosperm forest communities gradually rose to dominance in both uplands and lowlands along with other diverse plant communities, indicating the establishment of the Mesophytic Flora.

Keywords: Permian–Triassic, floral changeover, Paleophytic–Mesophytic transition, continental ecosystem, North China

INTRODUCTION

The response of plant communities to the Permian–Triassic mass extinctions is much debated (e.g. Cascales-Miñana et al., 2016; Nowak et al., 2019). There is no doubt that global floras changed substantially during the Permian–Triassic transition, from the Paleophytic Flora of the late Paleozoic to the Mesophytic Flora of the Mesozoic (Niklas et al., 1983; Cleal and Cascales-Miñana, 2014), but details of the timing are uncertain because of the absence of a robust stratigraphic framework in many terrestrial sections. Regional-scale paleobotanical and palynological work has suggested variable responses to the crisis. Palynological data from East Greenland initially suggested a significant change amongst land plants, especially the disappearance of conifers, followed by delayed recovery (Looy et al., 1999, 2001). Other studies have suggested that there is no extinction in palynological records around the Permian–Triassic Boundary (Hochuli et al., 2016; Schneebeli-Hermann et al., 2017). In Australia and South Africa, a clear extinction is marked by the disappearance of the *Glossopteris* flora (Fielding et al., 2019; Vajda et al., 2020; Mays et al., 2020; Gastaldo et al., 2020; McLoughlin et al., 2021). Data from South China show a considerable loss of land plants during the Permian–Triassic mass extinction (Xiong and Wang, 2011; Yu et al., 2015; Feng et al., 2020; Chu et al., 2020). The changes of macro-plant fossil assemblages from the Permian to Triassic of North China is clear (Wang, 1993; Wang, 2010; Stevens et al., 2011; Lu et al., 2020) but its link with the crisis is uncertain.

The Permian–Triassic mass extinction (252 Ma) was the most severe biotic crisis in the Phanerozoic, and was associated with highly-stressed conditions due to a combination of proposed factors such as global warming (Sun et al., 2012; Benton, 2018; Frank et al., 2021), acid rain (Sephton et al., 2015), wildfires (Shen et al., 2011;

Chu et al., 2020), increased UV-B flux (Visscher et al., 2004; Foster and Afonin, 2005), atmospheric heavy metal pollution (Hochuli et al., 2017), increase of continental weathering (Song et al., 2015; Lu et al. 2020) and strong volcanic activity (Wignall, 2015; Benton, 2018). The crisis eliminated over 80% of marine species, 70% of terrestrial vertebrate species and more than 50% of plant genera, including 42% of lycophytes and ferns, and 70% of gymnosperms, and was followed by the Early Triassic coal gap (Niklas et al., 1983; Retallack et al., 1996; Rees, 2002; Benton, 2014; Cascales–Miñana et al., 2016; Stanley, 2016; Dal Corso et al., 2022).

Here we present an investigation of some groups of continental organisms using a recently refined age model for the Permian to Middle Triassic in North China. Five successive floras are established in association with corresponding vertebrate and invertebrate faunas, which record substantial changes in continental ecosystems during the Paleophytic–Mesophytic transition.

GEOLOGICAL SETTING

During the Permian, six paleofloras were developed in different paleophytogeographical provinces (Chaloner and Lacey, 1973; McLoughlin, 2001, 2011), but during the Early Triassic, provincialism was reduced and a more cosmopolitan lycopsid flora occurred over most of the Northern Hemisphere, while *Dicroidium* forests and locally abundant isoetalean and pleuromeian lycopsids covered the Southern Hemisphere (Fig. 1A). North China, with its Permian Cathaysian Flora, traversed low latitudes (about 30°N), drifting north towards the north-eastern part of the Paleo-Tethys Ocean during the late Paleozoic and early Mesozoic (Fig 1A; Wang et al., 1998). Sedimentary sequences suggest there was a

large lake, about 1400 km wide, in North China during the Permian–Triassic (Fig 1B, C; Zhu et al., 2007; Liu et al., 2015; Ji et al., 2021, 2022).

The Permian to Middle Triassic succession in North China is divided into the Upper Shihhotse, Sunjiagou, Liujiagou, Heshanggou and Ermaying formations. The Upper Shihhotse Formation is dominated by grayish yellow/green sandstone with varicolored (dark red dominated) mud-siltstone. The Sunjiagou Formation comprises red thin- to medium-bedded mudstones with some red sandstones and interbedded calcareous nodules; the overall association is interpreted as a fluvial and floodplain system (Zhu et al., 2007; Zhu et al., 2020; Ji et al., 2022). Intermittent marine flooding occurred, indicated by some marine fossils in the upper part of the formation in the southwestern part of the study region (Yin and Lin, 1979; Chu et al., 2019). The overlying Liujiagou Formation is composed of massive red sandstones with a few interbedded mud-siltstones, locally bearing wrinkle structures, usually taken as evidence of microbial mats (Chu et al., 2015; Tu et al., 2016). There are mud cracks and ripple marks in the lower part, and some large sand sheets interbedded with thick conglomerates in the middle–upper part. This unit was deposited in various fluvial or lake-shore environments (Zhu et al. 2020; Ji et al. 2022). The Heshanggou Formation consists of red siltstones interbedded with some thin sandstone beds and abundant calcareous nodules, interpreted to have formed in shallow lakes (Hu et al., 2009). The Ermaying Formation comprises grayish green, thick-bedded sandstones with green and red thin-bedded mudstones and was deposited in fluvial-lacustrine settings. Abundant fossil plants and sporomorphs have been identified from various locations (Fig. 1D and Supplementary Data File 1).

The ages of the studied formations have been discussed for a long time, and are derived from isolated fossils, magnetostratigraphy, chemostratigraphy and a few U-Pb

dates from ash beds. A recent U-Pb zircon study (Wu et al., 2021) shows that most of the Upper Shihhotse Formation is of latest Asselian to early Kungurian age (294.8 ± 1.2–≤ 280.73 ± 0.12 Ma) rather than Guadalupian–early Lopingian as previously thought, although its uppermost part may still be latest Capitanian–Lopingian (≤ 261.75 ± 0.29 Ma). Most of the Guadalupian seems to be absent in parts of North China in this new dating scheme (Wu et al., 2021) whilst the magnetostratigraphy of the uppermost Upper Shihhotse Formation indicates a Wuchiapingian age (Guo, 2022). The negative carbon isotope excursions in organic matter ($\delta^{13}C_{org}$) in the middle part of the Sunjiagou Formation provides a potential marker for a latest Changhsingian age (Wu et al., 2020) and a mixed marine-continental fauna marking the Permian–Triassic transitional beds was identified in the middle–upper part of the Sunjiagou Formation (Chu et al., 2019). A CA-ID-TIMS U-Pb age of 252.21 ± 0.15 Ma from the middle part of the Sunjiagou Formation in the Shichuanhe section also suggests a latest Changhsingian age for the middle part of the Sunjiagou Formation (Guo et al., 2022). Thus, the Permian–Triassic boundary (PTB) lies in the upper part of the Sunjiagou Formation according to carbon isotope stratigraphy, biostratigraphy and magnetostratigraphy (Chu et al., 2017; Shu et al., 2018; Guo et al., 2019; Wu et al., 2020; Lu et al., 2020; Guo et al., 2022). The basal beds of the overlying Liujiagou Formation yield the *Aratrisporites-Alisporites* sporomorph assemblage (Ouyang and Zhang, 1982; Ouyang and Wang, 1985), and the lycopsid *Pleuromeia* occurs in the upper part of the Liujiagou Formation (Wang and Wang, 1982), all indicating an Early Triassic age (Wang, 1993; Shu et al., 2018; Guo et al., 2019), as does an LA-ICP-MS age of 251 ± 4 Ma from the middle part of the Liujiagou Formation (Zhu et al., 2019). Magnetostratigraphy suggests the Induan–Olenekian boundary is found in the lower part of the Liujiagou Formation (Guo et al., 2022). The Heshanggou

149 Formation yields abundant trace fossils together with body fossils (e.g., fossil plants,
150 vertebrates, fishes, conchostracans (= diplostracans) and ostracodes) of late Early
151 Triassic age (Wang et al., 1978; Qu et al., 1983; Nesbitt et al., 2011). Moreover,
152 magnetostratigraphy confirms an Olenekian age for the Heshanggou Formation (Guo
153 et al., 2022). An ID-TIMS U-Pb zircon date of 243.528 ± 0.069 Ma dates the upper
154 member of the Ermaying Formation as Anisian (Middle Triassic) (Liu et al., 2018).
155 Magnetostratigraphy indicates the Olenekian–Anisian boundary occurs in the basal
156 Ermaying Formation (Guo et al., 2022).

157 Here, we focus on five Permian–Triassic sections that yield well-preserved fossil
158 plants: the Liulin, Peijiashan, Dayulin, Shichuanhe and Zishiya sections (Fig. 1B, C;
159 Fig. 2). In addition, we also mention some other fossil sites with rich plant fossils,
160 such as Heshun, Pingyao and Yushe in Shanxi Province. In the following account, we
161 first focus on the biotas. The potential taphonomic issues that might bias the results
162 will be detailed in the discussion.

163

164 **MATERIALS AND METHODS**

165 This study is mainly based upon over 1400 plant megafossil specimens collected
166 from eight locations ranging through all the target formations in North China (Table
167 1). These include compression, impression and permineralized fossils. The fossils
168 represent shoots, leaves, cones or fertile parts and some trunks/fossil woods, most of
169 which were identifiable. We also restudied all reported fossils from North China and
170 in total we note 52 genera of vertebrates, 42 genera of invertebrates, 102 genera and
171 some form types of plants from over 120 locations (Supplementary Data Files 1–7). In
172 addition, some well-preserved cuticles were prepared by HF/HCl maceration and
173 Schultze solution for oxidation, and KOH to remove remnant humic acids (Kerp,

1990; Jones and Rowe, 1999). *In situ* pollen from male cones or fertile shoots were processed by HF/HCl maceration (Jones and Rowe, 1999). All fossils studied are stored in the paleontological collection of the State Key Laboratory of Biogeology and Environmental Geology, China University of Geosciences (BGEG, Wuhan).

Plant megafossil specimens were photographed using a Canon EOS 7D digital camera, and some *in situ* pollen, bract-scale complexes, small shoots and conchostracan specimens were examined and photographed using a LEICA-DM-750P microscope equipped with an automatic camera image stacking system. Some photos were processed by focus stacking methods using Photoshop CS5 (auto-align layers and auto-blend layers). Some *in situ* pollen were studied using a Hitachi SU8010 scanning electron microscope. In addition, one tetrapod tooth fossil from the uppermost Upper Shihhotse Formation and one well-preserved strobilus of *Pleuromeia* from the Liujiagou Formation were scanned using a nanoVoxel 4000 micro-computed tomography scanner (Sanying Precision Instruments, Tianjing, China) and the raw projections were converted into image stacks using VoxelStudio Recon (Sanying Precision Instruments). The isometric voxel size (spatial resolution) for the *Pleuromeia* and the tooth were 31.60 μm and 17.63 μm, respectively. To image the inner structure of the tooth, its volume data were segmented using the watershed algorithm in Avizo 8.0, and manual correction was performed to correct defects.

For paleoecological analysis, we normalized genera of fossil plants as binary data, present (1) or absent (0), in each formation (Cleal et al., 2021). The presence-absence matrix was then analyzed in R by hierarchical clustering using the Euclidean complete method, *k*-means clustering and principal components analysis (PCA) (Fig. S3–5). The R code is provided in the Supplementary material. To calculate the

hygrophyte(H)/xerophyte(X) ratio, plant genera were classified as hygrophytes, mesophytes and xerophytes based on previous studies (Supplementary data files 9 and 10) and then the ratio calculated as [H/(H+X)]/[X/(H+X)] (DiMichele et al., 2020; Koll and DiMichele, 2021; Supplementary datafile 10).

MACROFLORAS FROM PERMIAN TO MIDDLE TRIASSIC IN NORTH CHINA

Based on collected specimens and previously reported data, five successive macrofloras were identified from the Permian to Lower Triassic in North China. Previously, most of the floras were named after the formations in which they occurred, but here we consistently refer to them based on the index fossils because some of the floras span more than one formation. The gigantopterid flora in the Upper Shihhotse Formation has been well-studied previously (Wang, 2010; Stevens et al., 2011) and we confirm those earlier results. Here we focus on the other four macrofloras, i.e. the Voltziales flora in the uppermost part of the Upper Shihhotse and the Sunjiagou formations, the *Pleuromeia–Neocalamites* flora in the middle–upper part of the Liujiagou and the base of the Heshanggou formations, the *Pleuromeia–Tongchuanophyllum* flora in the lower–upper part of the Heshanggou and the basal part of the Ermaying formations, and the *Lepacyclotes–Voltzia* flora in the lower to upper parts of the Ermaying Formation.

The Voltziales flora

This flora occurs in the uppermost part of the Upper Shihhotse Formation and the lower part of the Sunjiagou Formation. It is dominated by Voltziales conifers, including walchian and voltzian voltzialean type conifers. Here the Voltziales flora is

subdivided into the ginkgophyte–walchian Voltziales and the voltzian Voltziales subfloras.

The ginkgophyte–walchian Voltziales subflora

This subflora occurs in the uppermost part of the Upper Shihhotse Formation of the Liulin (Fig. 2; Fig. S1B) and Shichuanhe sections (Fig. 2; Fig. S1C). It is dominated by walchian voltzialean shoots, other vegetative-shoot types of conifers (form type 0, 2 and 5, in Supplementary Data File 2), and includes ginkgophytes (form type 1 and 2, in Supplementary Data File 2), pteridosperms (*Autunia*), putative cycadophytes (*Taeniopteris*) and *Sphenopteris*-type foliage (Fig. 3). Gymnosperms are the main elements in this subflora. In the uppermost Upper Shihhotse Formation of the Liulin section, over 80% of plant fossils are shoots and leaves, whereas seed fossils account for about 20%. Around 85% of the shoot compressions/impressions are assigned to conifers and most of these conifer shoots are walchian Voltziales according to their gross morphology and cuticles (Fig. 3, description in Supplementary Data File 2). Some ginkgophyte leaves and *Taeniopteris* locally co-occur with the conifer shoots. In the uppermost Upper Shihhotse Formation of the Shichuanhe section, 385 specimens were collected and 256 identified. Among these, over 65% are assigned to conifer shoots, about 25% are ginkgophyte leaves, and there are a few *Autunia*-type pteridosperm ovuliferous organs, noeggerathialean leaves and other foliage types. In addition, there are some *in situ* monosaccate pollen associated with walchian voltzialean shoots that are elliptical to circular in polar view (Fig. 3X, Y), showing a monolete suture on the corpus, a punctate or in some cases rugulate surface. These are assigned to *Potonieisporites*. This subflora is named the ginkgophyte–walchian Voltziales subflora, after its two dominant elements.

The voltzian Voltziales subflora

This subflora of the Voltziales flora was identified from the lower part of the Sunjiagou Formation in the Liulin (Fig. 2; Fig. S1E), Dayulin (Fig. 2; Fig. S1F) and Zishiya (Fig. 2; Fig. S1G) sections. It is dominated by conifers, including *Pseudovoltzia*-type/ *Ullmannia*-type/ other undefined vegetative shoots with well-preserved cuticles (form type 1–4, description in Supplementary Data File 2), *Pseudovoltzia*-type bract-scale complexes with five-lobed scales (Fig. 4AA), male cones with *in situ* monolete bisaccate pollen of the *Gardenasporites*-type (Fig. 4DD, EE, PP, SS) and seeds, with some pteridosperms, such as *Autunia*-type peltate ovuliferous organs and *Germaropteris*-type vegetative small leaves with well-preserved cuticles (Fig. 4, description in Supplementary Data File 2). Calamite stems occur sporadically as compressions or impressions. In the lower part of the Sunjiagou Formation of the Liulin section, 220 discernible specimens were found, 76% of which are shoots, 11% seeds and 13% fertile parts. Around 96% of the shoot compressions/impressions can be assigned to conifers and 4% to ferns and pteridosperms. In the lower part of the Sunjiagou Formation of the Dayulin section, 37 identifiable specimens were collected, all of which are conifer shoot compressions and isolated conifer leaf compressions. In addition, there are over 300 specimens from the lower part of the Sunjiagou Formation of the Zishiya section and 202 of these were identifiable. Of these, shoots comprise about 70%, seeds around 19%, fertile parts (including cones) about 8%, and a few stems about 3%. All shoots and one cone can be assigned to conifers, the other fertile parts to the *Autunia* type, a few stems to *Calamites*, and some dispersed seeds to conifers or pteridosperms. This subflora is named after the dominant element as the voltzian Voltziales subflora.

The *Pleuromeia–Neocalamites* flora

Only a few localities, such as Jiaocheng, Yushe and Heshun in Shanxi, yield these plant fossils. They come from the middle-upper part of the Liujiagou Formation and the base of the Heshanggou Formation (Fig. 2). Most of these plant fossils are strobili, isolated sporophylls and rhizomorphs of *Pleuromeia jiaochengensis* and *Pleuromeia sternbergii* (Figs. 5C–K, 6A–D, M). Numerous fragments of *in situ* stems of *Neocalamites* or *Equisetites* preserved as compressions or casts also occur in both red silty mudstones and gray-green siltstones (Figs. 6E–K). Fragments of strap-shaped leaves with parallel veins are possible gymnosperms. Some fragments of sporophylls with long tips characteristic of *Tomiostrobus* were found at the base of the Heshanggou Formation at Heshun (Fig. 6L). In addition, some broken fronds of *Scolopendrites* (Figs. 5A–B) and some dispersed possible male cones, bract-scale complexes and seeds of voltzialean conifers (Figs. 6N–O) occur in this flora. Potential cycadophytes are identified as *Taeniopteris*. This flora is named after the two dominant elements, *Pleuromeia* and *Neocalamites*. *Pleuromeia* by itself is not diagnostic of an individual flora as its stratigraphic range extends into the overlying *Pleuromeia–Tongchuanophyllum* and *Lepacyclotes–Voltzia* floras (see below).

The *Pleuromeia–Tongchuanophyllum* flora

Abundant fossil plant specimens occur in the lower–upper part of the Heshanggou Formation and the basal part of the Ermaying Formation in the Yushe, Pingyao and Puxian sections in Shanxi. Numerous plant fossils have been previously reported from this interval from many other localities, such as Shouyang, Pingyao, Puxian, Fengfeng, Chengde, Jiyuan, and Yima (Supplementary Data Files 2–3). Most

of them are lycophytes, e.g., *Pleuromeia epicharis*, some stems with very small leaf cushions *Mesolepidodendron*, some sporophylls with long tips of *Tomiostrobus* (Figs. 7A–D, G, H, J–L), and pteridosperms (up to nine genera, e.g., *Tongchuanophyllum*, *Neoglossopteris*, "*Gangamopteris*", *Glossophyllum*, "*Euryphyllum*", *Scytophyllum*, "*Thinnfeldia*", *Sphenopteris* and *Peltaspermum*) (Figs. 7M–O), and the others are sphenophytes (e.g., *Neolobatannularia*, *Phyllotheca*, *Neocalamites*, *Equisetites*) (Figs. 7I), pteridophytes (e.g., *Anomopteris, Scolopendrites, Neuropteridium, Todites*), conifers (*Voltzia*, *Yuccites*, *Willsiostrobus*) (Figs. 7P–Q), and putative cycadophytes (possibly *Cycadocarpidium*) (Supplementary Data File 2, 3). This flora is named after its abundant lycopods, dominated by *Pleuromeia*, and the common occurrence of *Tongchuanophyllum*.

The *Lepacyclotes–Voltzia* flora

This flora occurs in the lower to upper parts of the Ermaying Formation where the Mesophytic floral elements gradually appear and become more diverse. However, some lycophyte rhizophores (*Pleuromeia*), some lycophyte sporophylls with short tips (*Lepacyclotes*), *Isoetites*, and sphenophytes (*Neocalamites* and *Equisetites*) remain common but sphenophyte stems became larger than those in the former floras (Fig. 8). Fronds and pinnules of true ferns from the lower to upper parts of the Ermaying Formation were identified as *Anomopteris*, *Cladophlebis*, *Danaeopsis*, *Symopteris* (*Bernoullia*) and *Todites* (Supplementary Data File 2, 3). In addition, there is a diverse flora of pteridosperms (e.g., *Germaropteris*, *Peltaspermum*, *Ptilozamites*, *Glossophyllum*, *Neoglossopteris*, *Scytophyllum*, *Tongchuanophyllum*, "*Thinnfeldia*", *Pachypteris* and *Protoblechnum*), cycadophytes (e.g., *Nilssonia*, *Sinozamites* and *Taeniopteris*), ginkgophytes (e.g., *Baiera*, *Ginkgoites* and *Sphenobaiera*) and conifers

(e.g., *Pagiophyllum*, *Podozamites*, *Voltzia* and *Yuccites*) (Supplementary Data File 2, 3). This flora is named after the common Middle Triassic elements, *Lepacyclotes* and *Voltzia*.

DISCUSSION

Ages of the Lopingian to Middle Triassic macrofloras in North China

The floras of North China can be dated with reference to other fossils such as vertebrates. The ginkgophyte–walchian Voltziales subflora of the uppermost Upper Shihhotse Formation of the Shichuanhe and Liulin sections co-occurs with a vertebrate tooth fossil (Fig. 9A–D) of the Jiyuan fauna (Fig. S2; Xu et al. 2015). The Jiyuan Fauna comprises abundant vertebrate taxa (Supplementary Data file 7; Xu et al. 2015) that are assigned a Wuchiapingian age based on comparisons of the entire tetrapod assemblage to the Ilinskoe Subassemblage of the Sokolki Assemblage in Russia and the *Cistecephalus* Assemblage Zone in South Africa (Liu et al. 2014; Benton 2016). A Wuchiapingian age of the strata is also supported by magnetostratigraphy (Guo, 2022).

Previously a *Ullmannia bronnii–Yuania magnifolia* assemblage was documented by Wang and Wang (1986) from the lower–middle part of the Sunjiagou Formation of North China. Unfortunately, we have not collected any *Yuania* in these strata during our reinvestigation (Supplementary Data file 2–3), thus herein we use the term *Ullmannia–Pseudovoltzia–Germaropteris* assemblage as a replacement name. The *Ullmannia–Pseudovoltzia–Germaropteris* assemblage corresponds to the voltzian Voltziales subflora. This subflora and the corresponding *Lueckisporites virkkiae–Jugasporites schaubergeroides* sporomorph assemblage (Hou and Ouyang, 2000) co-occur with a *Pseudestheria* (Fig. 9H–K) conchostracan assemblage in the Liulin and

Dayulin sections (Figs. 2, 9, S2), which is assigned to the Lopingian (probably Changhsingian). In North China, some pareiasaurs (Wang et al., 2019) and fish fossils (Chondrostei and *Platysomus*) (Wang, 1981) were reported from the Sunjiagou Formation and the laterally equivalent Naobaogou Formation (Liu and Bever, 2018, Fig. S2, Supplementary Data file 7). In addition, the *Darwinula–Panxiania* ostracod assemblage occurs in the middle part of the Sunjiagou Formation (Chu et al., 2015, Fig. S2, Supplementary Data file 5). Further, mixed continental-marine biotas (Fig. 9), comprising conchostracans, plants, insects, marine bivalves and lingulid brachiopods, in the middle part of the Sunjiagou Formation are particularly important for biostratigraphic correlation between continental and marine facies (Chu et al., 2019). All the floral data suggest the Permian–Triassic transitional beds start in the middle part of the Sunjiagou Formation. This is further supported by a CA-ID-TIMS U-Pb age of 252.21 ± 0.15 Ma from the middle part of the Sunjiagou Formation in the Shichuanhe section (Guo et al., 2022).

However, some pareiasaurs were also found from the uppermost part of the Sunjiagou Formation at the Xuecun section, Liulin, Shanxi Province (Wang et al., 2019, Fig. S2, Supplementary Data file 7). Pareiasaurs from the continental sections in Russia and South Africa are not considered to have survived the Permian–Triassic mass extinction (Lee, 1997; Benton, 2016). Meanwhile, abundant microbial-induced sedimentary structures (MISS), such as wrinkle structures, appear in the top part of the Sunjiagou Formation and lower part of the Liujiagou Formation at Dayulin (Yiyang, Henan Province), and are common in post-extinction environments (Chu et al., 2015; Tu et al., 2016), as seen in high southern latitudes (Mays et al., 2021a, b). Consequently, the age of the upper part of the Sunjiagou Formation is unclear. The uncertainty over the age of the top of the Sunjiagou Formation may be because the

transition with the overlying Sunjiagou Formation is diachronous. An *Aratrisporites–Alisporites* sporomorph assemblage, in which *Aratrisporites* is the most abundant element (13.4%), and *Alisporites* is a sub-dominated element (10.3%), occurs with a few fragmentary fossils of *Dicynodon* in the lower part of the Liujiagou Formation (Ouyang and Zhang, 1982, Fig. S2, Supplementary Data file 7), indicating an earliest Triassic (Induan) age. This conclusion is further supported by magnetostratigraphy that indicates a likely Dienerian age for this level (Guo et al., 2022).

In the middle part of the Liujiagou Formation in the Peijiashan section and the base of the Heshanggou Formation in the Shichuanhe, Heshun and Yushe sections, the *Pleuromeia–Neocalamites* flora co-occurs with a conchostracan *Leptolimnadia–Paleoleptestheria* assemblage and some Triopsidae (Fig. S2, Supplementary Data file 5; Tong et al., 2018). Furthermore, from the lower–middle part of the Qishan Formation (equivalent to the Liujiagou Formation) of the Zishiya section, we found a *Lundbladispora–Cycadopites–Protohaploxypinus* sporomorph assemblage that can be correlated to the *Densoisporites nejburgii–Lunatisporites–Cycadopites* sporomorph assemblage (Qu et al., 1980; Qu et al., 1982; Tong et al., 2018). There are also some bivalves, some ophiurids and the *Leptolimnadia–Paleoleptestheria* conchostracan assemblage in the Qishan Formation (Fig. 9G, R, Supplementary Data file 5; Tong et al., 2018), all of which indicate an early Olenekian age.

Subsequently, the lower part of the Heshanggou Formation is characterized by the *Pleuromeia–Tongchuanophyllum* flora that is associated with a few tetrapod fossils (e.g., Capitosauridae) (Wang, 1983) and the *Cornia–Estheriella* conchostracan assemblage (Wang, 1983). Higher up in the middle–upper parts of the Heshanggou Formation and basal Ermaying Formation, sporomorphs are assigned to the *Lundbladispora–Verrucosisporites–Lunatisporites* sporomorph assemblage and occur

along with the macroflora documented above (Qu et al., 1980; Ouyang and Norris, 1988; Tong et al., 2018). The sporomorph assemblage includes a higher proportion of gymnosperm pollen (*Cycadopites* and *Lunatisporites*) (Ouyang and Norris, 1988). In addition, vertebrate fossils (including the lungfish *Ceratodus heshanggouensis*) increase in abundance (Wang, 1983, Supplementary Data file 7). Among invertebrates, abundant conchostracans of the *Magniestheria–Eosolimnadia* assemblage occur, together with abundant ostracod fossils of the *Darwinula triassiana–Darwinula fengfengensis–Darwinula rotundata* assemblage (Supplementary Data file 5, Pang, 1989; Tong et al., 2018). Thus, the age of most of the Heshanggou Formation should be Olenekian, except the uppermost part that hosts the *Shaanbeikannemeyeria* assemblage, which is assigned an Anisian age (Liu, 2018; Fig. S2, Supplementary Data file 7).

Finally, in the Ermaying Formation, the *Lepacyclotes–Voltzia* flora is associated with the *Punctatisporites–Chordasporites* sporomorph assemblage (Tong et al. 2018, Fig. S2, Supplementary Data file 2–3). It co-occurs with abundant vertebrate and invertebrate fossils, i.e., the *Sinokannemeyeria–Parakannemeyeria–Shansiodon* tetrapod assemblage (Liu and Sullivan 2017; Liu et al., 2018, Fig. S2, Supplementary Data file 7), the *Brachyestheria–Xiangxiella* conchostracan assemblage (Tong et al. 2018), and the *Lutkevichinella minuta–Shensinella gaoyadiensis–Darwinula subovaliformis* ostracod assemblage (Tong et al. 2018, Fig. S2, Supplementary Data file 5). This biota indicates an Anisian age.

Permian to Middle Triassic floral changes

The Permian-Triassic mass extinction was the most severe event of the Phanerozoic, affecting both marine and continental organisms (Cascales-Miñana et al.

2016; Dal Corso et al., 2022). However, it has been even debated whether there was a mass extinction of land plants (Fielding et al., 2019; Nowak et al., 2019). In North China, it is well known that Permian lands were occupied by the famous *Gigantopteris* (Cathaysian) flora, which gradually went extinct in the later Permian (Hilton and Cleal, 2007; Wang, 2010; Stevens et al., 2011; Wu et al., 2021). There have been few investigations of paleofloral changes at other intervals through the Permian, Early and Middle Triassic (Wang, 1993, 1996; Wang, 2010; Stevens et al., 2011; Yang et al., 2012). A statistical analysis has been especially lacking. Here, we identify six statistically-distinct floras through this interval (Figs. 10–12), separated by five floral transitions (T1–T5 in Fig. 10). Of these distinct floras, two are similar to each other, and they are regarded as the sub-floras of one flora. These changes may help us to understand the Permian–Triassic transition of the plants on land in North China. In some instances, floral transitions are abrupt and can be well-defined by changes in composition at a particular level (represented by horizontal lines in Figure 10). In other cases, the transitions span a broader time interval which may, in part, be due to low sampling frequency.

The first significant floral transition (T1) is recognized between the gigantopterid and Voltziales floras (Fig. 10, 11B (a)). The gigantopterid flora was characterized by high diversity, including abundant and diverse gigantopterids, arborescent lycophytes, diverse sphenophytes and “filicalean” ferns, abundant ginkgophytes, Noeggerathiales and Cordaitales but with few conifers. During this transition (Fig. 11B, from cluster 1 to cluster 2 and from cluster 2 to cluster 3) there is a decrease or the eventual loss of the dominant/characteristic elements, e.g., gigantopterids (Fig. 10). It is characterized by the disappearance of the Cathaysian flora (Wu et al. 2021) and a switch from the Cisuralian gigantopterid flora to the Lopingian Voltziales flora. This also marks the

449 beginning of the Paleophytic to Mesophytic floral switch, which is a staggered event
450 in our analysis. T1 marked the decline and eventual extirpation (regional extinction)
451 of the gigantopterid flora (61.8% genera lost) and replacement by the incoming
452 Voltziales flora that comprises taxa that ranged through this selective extinction event.
453 The second floral transition (T2) occurs within the Voltziales flora and is
454 manifested as the turnover between the two subfloras (Fig. 10, 11) in which 10 taxa
455 disappear, 2 appear and 11 range through the transition. The ginkgophyte–walchian
456 Voltziales subflora (Fig. 10, 11) is dominated by abundant walchian voltzialean
457 conifers and early ginkgophytes, together with the cycad *Taeniopteris*, some
458 pteridosperms (e.g., *Sphenopteris*, *Autunia*, *Supaia*), sphenophytes (e.g.,
459 *Sphenophyllum*), remaining ferns (e.g., *Pecopteris*), a few Noeggerathiales (e.g.,
460 *Yuania*) and a limited appearance of voltzian voltzialean conifers. Overall, the
461 subflora is dominated by gymnosperms (>90%), rather than ferns, and it fits the broad
462 characteristics of the 'Mesophytic age' (Gothan 1912; DiMichele et al., 2008). It is
463 relatively different from the older gigantopterid-dominated flora in North China. So, it
464 may be correlated with previously reported floras from the Upper Shihhotse
465 Formation, such as the upper part of the *Psygmophyllum* zone (Wang, 1993), the post-
466 changeover 4 flora (Wang, 2010) or the post-uUSF extinction flora (Stevens et al.,
467 2011) (Fig. 10). However, there are some differences in the dominant elements in two
468 subfloras of the Voltziales flora. The voltzian Voltziales subflora (Fig. 10, 11) is
469 dominated by voltzian voltzialean conifers, some pteridosperms, and a few
470 sphenophytes and ferns. The presence of a diverse voltzian Voltziales assemblage
471 with a few walchian Voltziales but no early ginkgophytes is especially noteworthy.
472 The third transition (T3) is more difficult to characterize and interpret as it
473 comprises two stages separated by a broad interval lacking plant megafossils from the

Terrestrial ecological disturbance interval (TED interval) (see Xu et al., 2022). T3 commences with the disappearance of the latest Permian voltzian Voltziales subflora with 10/13 loss in genera across a wide range of plant groups (Figs. 10, 11B (b)). This transition event (T3) can be probably regarded as the end Permian plant extinction (EPPE) (Xu et al., 2022) and the PTB plant mass extinction in North China, but it spans a wide time interval due to low sampling frequency (Fig. 10) and is best evidenced by the incoming Early Triassic flora. However, the duration of the crisis could be affected by poor preservation at this level in the TED interval. The dominantly red beds of mudstone and sandstone floodplain facies of the upper part of the Sunjiagou Formation provide a poor fossil plant record (see DiMichele et al., 2008). Such a scenario is supported by the absence of disaster floral elements such as *Pleuromeia*, which appears at a higher level, in the Liujiagou Formation, and the presence of pareiasaurs in the Sunjiagou Formation (Wang et al., 2019; Supplementary Data file 7) which suggests sufficient vegetation existed to support herbivorous vertebrates. Furthermore, the palynoflora from the basal Liujiagou Formation includes the voltzialean conifer pollen *Triadispora* (see Balme, 1995), suggesting that even though the voltzialean-dominated community disappeared in the megafossil record, the group was still present in the region. Plants from this community may not necessarily have been living in the floodplain depositional settings as conifer pollen is widely distributed (Ouyang and Zhang, 1982).

Following the initial loss of plant diversity in T3, the first megaflora of the Early Triassic, the *Pleuromeia–Neocalamites* flora (Fig. 12), is characterized by abundant *Pleuromeia* (typically *Pleuromeia jiaochengensis*) and common sphenophyte stems (*Neocalamites* and *Equisetites*) along with some pteridophytes and a few voltzian conifers (Fig. 10). We consider the appearance of this megaflora to mark the end of

the third transition event (T3) (Fig. 10). An alternative interpretation might be to divide the T3 event as presented here into a separate late Permian extinction event and an earliest Triassic radiation event. While future research is required to fully evaluate floral changes in transition, we consider this scenario less likely as the extinction and radiation appear intricately linked to the environmental perturbations of the TED interval.

The fourth floral transition (T4), from the *Pleuromeia–Neocalamites* to *Pleuromeia–Tongchuanophyllum* floras (Figs. 10, 11A), represents a radiation event and short-term increase in gymnosperm diversity after the crisis in North China, characterized by the abrupt rise of pteridosperms and a few cycadophytes and conifers. The diversity of *Pleuromeia* also increased noticeably, whereas sphenophytes and pteridophytes increased only slightly (Fig. 10). This transition spans a wide time interval, probably due to low sampling frequency.

Finally, the final floral transition (T5) from the *Pleuromeia–Tongchuanophyllum* to the *Lepacyclotes–Voltzia* floras (Fig. 10, 11B (c)) also spans a broad time interval due to low sampling frequency. In this radiation event many taxa co-occur in the *Pleuromeia–Tongchuanophyllum* and *Lepacyclotes–Voltzia* floras showing they are closely related to each other but are nonetheless distinct (Fig. 11). The latter flora is distinguished by a number of incoming pteridophytes, pteridosperms, cycadophytes, ginkgophytes and conifers. The *Lepacyclotes–Voltzia* flora shows full recovery from the Permian–Triassic crisis in terms of diversity and abundance of nearly all higher taxa, including lycophytes, sphenophytes, pteridophytes, pteridosperms, cycadophytes, ginkgophytes and conifers. Gymnosperms increased, especially ginkgophytes, cycadophytes and conifers, and pteridophytes also diversified as tree ferns and ground ferns (Figs. 10, 11, 12).

524 During the Lopingian, floral distributions were latitude-dependent (Fig. 1A;
525 Supplementary Data file 8), with four distinct floral provinces: the high-northern-
526 latitude *Cordaites* peat-forming flora of the Angaran province (Davydov et al., 2021;
527 Davydov and Karasev, 2021), the low-middle-northern-latitude voltzian Voltziales–
528 pteridosperm floras (e.g., the voltzian Voltziales subflora in North China; Bourquin et
529 al., 2011; Kustatscher et al., 2012, 2017; Cai et al., 2019), the tropical rainforest or
530 lowland-peat-forming floras (e.g., the *Gigantopteris* flora in South China or the Umm
531 Irna flora in Jordan; Yu et al., 2015; Blomenkemper et al., 2018; Feng et al., 2020)
532 and the high-southern-latitude *Glossopteris* peat-forming flora in Gondwana (Fielding
533 et al., 2019). During the Permian–Triassic mass extinction, floras changed
534 dramatically globally. Early Triassic floras were sporadically distributed but with
535 some widespread taxa (Fig. 1A). Herbaceous or shrub-like lycopsid-dominated floras,
536 mainly *Tomiostrobus* and *Pleuromeia*, were widely distributed in the northern
537 hemisphere (Fig. 1A; Supplementary Data file 8), and the *Lepidopteris*- and
538 *Dicroidium*-dominated flora became established in the southern hemisphere (Fig. 1A;
539 Supplementary Data file 8; Vajda et al. 2020).
540
541 **Evolution of terrestrial ecosystems from Permian to Middle Triassic in North**
542 **China**
543 Here we discuss the evolution of the ecosystems on land through the Permian–
544 Triassic transition, based on the fossil records of plants, sporomorphs, tetrapods,
545 fishes, invertebrates and trace fossils from North China. The transition was associated
546 with turbulent environmental changes (Fig. 13), some of which led to biological
547 responses, as highlighted by the hygrophyte/xerophyte ratio that reflects changes in

548 floral composition from wet (hygrophyte) to dry (xerophyte) ecological settings
549 (Supplementary Data file 9–10).

550 The subsidence of the Cisuralian gigantopterid-dominated rainforest
551 communities coincides with the last occurrence of coal deposits and the rise of the
552 Lopingian ginkgophyte–walchian Voltziales forest community (Fig. 12) in North
553 China. Disappearance of the *Gigantopteris* flora in North China represents a regional
554 loss of diversity and an extirpation event because many taxa, but not all, and the
555 *Gigantopteris* flora, persist in South China until the late Changhsingian where they
556 are notable victims of the EPPC (e.g., Yu et al., 2015; Feng et al., 2020, Xu et al.,
557 2022). In the meantime, the Jiyuan Fauna changed into the pareiasaur-dominated
558 fauna whilst insect diversity decreased (Fig. 13, Supplementary Data File 6–7; Xu et
559 al., 2015; Wang et al., 2019). The gradual changeover in the *Gigantopteris* flora
560 indicates increasing aridity, a trend that continues in the Voltziales flora (Fig. 13,
561 Supplementary Data file 9–10). A few insect remains (Fig. 9E) still co-occur with
562 conifers in the top of the Upper Shihhotse and Sunjiagou formations (Fig. 2), and then
563 there is no record of insect fossils from the point of disappearance of the
564 Changhsingian conifer forests to the Middle Triassic in North China (Zheng et al.
565 2018). Both plant macrofossils and sporomorph records in the lower–middle parts of
566 the Sunjiagou Formation were from voltzialean-dominated forests. The
567 hygrophyte/xerophyte ratio indicates that arid or semi-arid conditions prevailed
568 during the deposition of the lower–middle parts of the Sunjiagou Formation (Fig. 13).
569 The mean annual precipitation was calculated, based on the depth to the Bk horizon in
570 paleosols, as 320 ±147 mm/yr (Yu et al. 2022).

571 The disappearance of the voltzian Voltziales-dominated forests (T3; Fig. 12) in
572 the latest Changhsingian, is associated with the appearance of red beds commonly and

MISS in lacustrine facies (Chu et al. 2015). However, despite the apparent forest floral crisis of the EPPC, some tetrapods persisted in the Upper Sunjiagou Formation (Fig. 2, Liulin section; Fig. 13) as did aquatic invertebrates, such as the conchostracans *Palaeolimnadia* and *Euestheria* and ostracods *Darwinula* and *Panxiania* (Fig. 13, Supplementary Data File 5, 7, Chu et al., 2015). The Voltziales-dominated flora may have persisted in the latest Changhsingian, at the same time as the tetrapod losses, but poor preservation could have "back-smeared" the final occurrence.

The Early Triassic (Induan?) *Aratrisporites–Alisporites* sporomorph assemblage (Ouyang and Zhang, 1982) may represent the first herbaceous lycopsid plant community occupying lowlands, coexisting with a few upland gymnosperms (Fig. 12), established after the crisis. This was followed by the early Olenekian *Pleuromeia–Neocalamites* flora representing *Pleuromeia*/*Neocalamites*-dominated shrub marshes in muddy wetlands. These occur *in situ* in sandstones or silty mudstones of the Liujiagou Formation and the base of the Heshanggou Formation (Fig. S1H–I), interpreted as braided river and shallow lake environments (Ji et al. 2021). *Pleuromeia*/*Neocalamites*-dominated shrub marshes likely grew in riverbank or muddy floodplain settings. In the late stage of the *Pleuromeia–Neocalamites* flora, a few *Voltzia* conifer shrubs appeared and might have grown in well-drained sandy riverbanks. Some allochthonous fragments of *Tomiostrobus* may have been derived from sporadically distributed plants around small ephemeral water bodies. Concurrently, aquatic invertebrates appeared in this ecosystem, such as conchostracans, ostracods and Triopsidae (Wang, 1983). The hygrophyte/xerophyte ratio indicates a more humid environment in the early Olenekian than during the latest

Changhsingian in North China (Fig. 13, Supplementary Data file 9–10), which is consistent with geochemical data from paleosols in North China (Yu et al. 2022).

Subsequently, in the *Pleuromeia–Tongchuanophyllum* flora, pteridosperm–conifer shrub woodlands are identified by the appearance of abundant pteridosperms ("*Euryphyllum*", "*Gangamopteris*", *Glossophyllum*, *Neoglossopteris*, *Sphenopteris*, "*Thinnfeldia*", *Tongchuanophyllum*, *Peltaspermum* and *Scytophyllum*) and some *Voltzia* elements (Fig. 12). Lacustrine conditions were predominant in this stage (Hu et al., 2009). These *Voltzia*-dominated woodland communities grew in well-drained sandy-soil riverbanks or other lowlands (Fig. 12). The lycophyte (*Pleuromeia*)–sphenophyte (*Neocalamites*, *Equisetites* and *Phyllotheca*)-dominated shrub marsh community with some pteridophytes (e.g., *Todites*, *Neuropteridium* and *Anomopteris*) was still widely distributed on riverbanks or muddy floodplains (Fig. 12). Some *Tomiostrobus*-dominated, herbaceous, ground-covering communities occurred around the shores of playa lakes. In addition, some insect herbivory damage appeared on leaves of *Tongchuanophyllum* (Fig. 7O), and abundant small, spiral microconchid-like organisms on sporophylls of *Pleuromeia* (Fig. 7D) are preserved. Moreover, many vertebrate fossils (Benthosuchidae, Capitosauridae, Procolophonidae, Scaloposauria, *Eumetabolodon*, *Fugusuchus*, *Hazhenia*, *Pentaedrusaurus* and *Xilousuchus*), some fish (*Ceratodus*) and many invertebrates co-occur with this flora (Wang, 1983, Nesbitt et al., 2011, Fig. 13, Supplementary Data file 7). All these changes suggest that diverse terrestrial and aquatic ecosystems had begun to reappear (Fig. 12). At this time, there are abundant types of trace fossils in continental ecosystems (Fig. 13, Shu et al., 2018; Guo et al., 2019) recording widespread activity on land, as well as posture changes and the evolution of endothermy with insulation (hair, feathers) in synapsid and archosauromorph tetrapods (Benton, 2021). The increase of invertebrate

diversity (Fig. 13) may indicate a repopulation of aquatic ecosystems following their disappearance in the late Changxingian. Sporomorphs in the later stages of this flora are represented by the *Cycadopites–Lunatisporites–Verrucosisporites* sporomorph assemblage, and the hygrophyte/xerophyte ratio indicates a relatively seasonally humid environment in the late Olenekian (Fig. 13, Supplementary Data file 9–10) and the mean annual precipitation was calculated to range from 520 ±147 mm/yr to 680 ±147 mm/yr (Yu et al., 2022).

In the *Lepacyclotes–Voltzia* flora, some xerophytic gymnosperms (e.g., *Lepidopteris*, *Peltaspermum*, *Pagiophyllum*, *Yuccites* and *Voltzia*) started to occupy some dry uplands (Fig. 12) if they were not already established there; such absences may represent a taphonomic bias towards wetland depositional settings (see Blomenkemper et al., 2018). Along with the increased diversity of pteridophytes, pteridosperms, cycadophytes, ginkgophytes and conifers, the gymnosperm-dominated forest community started to occupy some dry uplands, and the pteridophyte-dominated shrub community entered moist lowlands. The *Pleuromeia*–sphenophyte-dominated shrub marsh community was still on riverbanks or muddy floodplains (Fig. 12). At that time, the *Sinokannemeyeria* fauna was widely distributed in North China (Liu and Sullivan, 2017). Aquatic invertebrates probably also increased (Figs. 12, 13), as also suggested by abundant burrows inside the cast of *Neocalamites* (Fig. 8F). The hygrophyte/xerophyte ratio indicates a gradual shift to a more humid climate (Fig. 13, Supplementary Data file 9–10).

CONCLUSIONS

A new integrated multifaceted biostratigraphic framework with a refined time scale is established for the Lopingian–Middle Triassic of North China, based on

647 macrofossil plant, sporomorph, vertebrate and invertebrate (conchostracans and
648 ostracodes) assemblages.

649 Five main floras are recognized are identified in North China, the gigantopterid,
650 Voltziales, *Pleuromeia–Neocalamites*, *Pleuromeia–Tongchuanophyllum* and
651 *Lepacyclotes–Voltzia* floras, with the Voltziales flora comprising the ginkgophyte–
652 walchian Voltziales and the voltzian Voltziales subfloras. The five transitions
653 between these floras consist of an extirpation event, two turnover events and two
654 radiation events. The gigantopterid flora regional extinction (T1; 34/55 genera lost)
655 eliminated the gigantopterid-dominated rainforest and saw the end of coal deposition
656 This marks the beginning of the changeover from the Paleophytic to Mesophytic
657 floras. The second floral transition (T2), is a subflora turnover within the Voltziales
658 flora, and saw a change in the dominant elements. The end-Permian plant extinction
659 event (EPPE; T3), which saw the loss of 10 out of 13 genera, marks the start of the
660 terrestrial ecological disturbance interval (TED interval) on land. This crisis was
661 followed by a short-term diversification (T4) from the *Pleuromeia–Neocalamites* to
662 the *Pleuromeia–Tongchuanophyllum* floras. The final floral transition (T5) in the
663 earliest Middle Triassic, indicating the recovery-radiation of plants, represented by the
664 *Lepacyclotes–Voltzia* flora, shows the initial construction of the Mesophytic Flora.

665 From the Cisuralian to Lopingian, the change from a gigantopterid-dominated
666 rainforest community to a voltzialean conifer forest community occurred in parallel
667 with the decline of the Jiyuan fauna and change to a pareiasaur-dominated fauna, loss
668 of coal deposits, sharp increase of red beds and aridity increase. The subsequent
669 disappearance of the voltzialean conifer forest community marks the end-Permian
670 plant extinction in North China. Following the prolonged plant-free Terrestrial
671 ecological disturbance interval the first plants to recover after the crisis belonged to a

672 herbaceous plant community, followed by a *Pleuromeia–Neocalamites* shrub marsh
673 community. A pteridosperm shrub woodland community dominated for a short time
674 in the late Early Triassic, along with the first appearance of insect herbivory. Finally,
675 in the Middle Triassic, the gymnosperm forest community gradually rose to
676 dominance with the appearance of diverse plant communities on lowland and possible
677 upland settings.
678
679 **ACKNOWLEDGMENTS**
680 This study was jointly funded by the National Natural Science Foundation of
681 China (grant numbers 9205520023, 42030513, 41661134047 and 41530104) and the
682 UK Natural Environment Research Council's Eco-PT project (NE/P01377224/1) to
683 P.B.W., M.J.B. and J.H. We thank our colleagues, Yuyang Wu, Yingyue Yu, Wenwei
684 Guo, Kaixuan Ji, Xue Miao, Meijia Zhang, Zhen Xu, Xin Sun, Qing Xue, Yuyang
685 Tian and Yan Ye for help in the field and general advice. Especially, we thank Patrick
686 Blomenkemper and Hans Kerp for guidance on cuticular analysis, Jacopo Dal Corso
687 for many constructive suggestions and Weidong Liu of Shanxi Institute of Geological
688 Survey for help with the reference "*Triassic of Shanxi*". We thank the editors Wenjiao
689 Xiao and Ganqing Jiang for their editions and reviews. In addition, we also thank four
690 anonymous reviewers for feedback on the manuscript.
691
692 **REFERENCES CITED**
693 Balme, B., 1995, Fossil in-situ spores and pollen grains: an annotated catalogue.
694 Review of Palaeobotany and Palynology 87, 81–323.

695 Blomenkemper, P., Kerp, H., Hamad, A.A., DiMichele, W.A., and Bomfleur, B.,
696 2018, A hidden cradle of plant evolution in Permian tropical lowlands. Science,
697 v. 362, p. 1414–1416.
698 Benton, M.J., and Newell, A.J., 2014, Impacts of global warming on Permo-Triassic
699 terrestrial ecosystems. Gondwana Research, v. 25, p. 1308–1337.
700 Benton, M.J., 2016, The Chinese pareiasaurs. Zoological Journal of the Linnean
701 Society, v. 177, p. 813–853.
702 Benton M. J., 2018, Hyperthermal-driven mass extinctions: killing models during the
703 Permian–Triassic mass extinction. Philosophical Transactions of the Royal
704 Society A, v. 376, p. 20170076.
705 Benton, M.J., 2021, The origin of endothermy in synapsids and archosaurs and arms
706 races in the Triassic. Gondwana Research, v. 100, p. 261–289.
707 Bourquin, S., Bercovici, A., López–Gómez, J., Diez, J.B., Broutin, J., Ronchi, A.,
708 Durand, M., Arche, A., Linol, B., and Amour, F., 2011, The Permian–Triassic
709 transition and the onset of Mesozoic sedimentation at the northwestern peri–
710 Tethyan domain scale: Palaeogeographic maps and geodynamic implications.
711 Palaeogeography, Palaeoclimatology, Palaeoecology, v. 299, p. 265–280.
712 Broutin, J., Roger, J., Platel, J. –P., Angiolini, L., Baud, A., Bucher, H., Marcoux, J.,
713 and Al Hasmi, H., 1995, The Permian Pangea. Phytogeographic implications of
714 new paleontological discoveries in Oman (Arabian Peninsula). Comptes Rendus
715 de l'Academie des Sciences Paris, Série Iia, v. 321, p. 1069–1086.
716 Broutin, J., Yu, J.X., Shi, X., Shu, W.C. and Qing, X., 2020, Terrestrial palaeofloral
717 succession across the Permian–Triassic Boundary in the North and South China
718 blocks: a brief review. Paläontologische Zeitschrift, v. 94, p. 633–644.

719 Cai, Y.F., Zhang, H., Feng, Z., Cao, C.Q., and Zheng, Q.F., 2019, A *Germaropteris*-
720 dominated flora from the upper Permian of the Dalongkou section, Xinjiang,
721 Northwest China, and its paleoclimatic and paleoenvironmental implications.
722 Review of Palaeobotany and Palynology, v. 266, p. 61–71.
723 Cascales–Miñana, B., Diez, J.B., Gerrienne, P., and Cleal, C.J., 2016, A
724 palaeobotanical perspective on the great end-Permian biotic crisis. Historical
725 Biology, v. 28, p. 1066–1074.
726 Chaloner, W.G., and Lacey, W.A., 1973, The distribution of Late Palaeozoic floras. p.
727 271–290 in Hughes, N.F. Ed., Organisms and continent through time. Special
728 Papers in Palaeontology, v. 12. Palaeontological Association, London.
729 Chu, D.L., Tong, J.N., Song, H.J., Benton, M.J., Bottjer, D.J., Song, H.Y., and Tian,
730 L., 2015, Early Triassic wrinkle structures on land: stressed environments and
731 oases for life. Scientific Reports, v. 5, p. 10109.
732 Chu, D.L., Tong, J.N., Benton, M.J., Yu, J.X. and Huang, Y.F., 2019, Mixed
733 continental–marine biotas following the Permian–Triassic mass extinction in
734 South and North China. Palaeogeography, Palaeoclimatology, Palaeoecology, v.
735 519, p. 95–107.
736 Chu, D.L., Grasby, S.E., Song, H.J., Corso, J.D., Wang, Y., Mather, T.A., Wu, Y.Y.,
737 Song, H.Y., Shu, W.C., Tong, J.N., and Wignall, P.B., 2020, Ecological
738 disturbance in tropical peatlands prior to marine Permian–Triassic mass
739 extinction. Geology, v. 48, p. 288–292.
740 Cleal, C.J., and Cascales-Miñana, B., 2014, Composition and dynamics of the great
741 Phanerozoic Evolutionary Floras. Lethaia, v. 47, p. 469–484.
742 Cleal, C.J., Pardoe, H.S., Berry, C.M., Cascales-Miñana, B., Davis, B.A.S., Diez, J.B.,
743 Filipova-Marinova, M.V., Giesecke, T., Hilton, J., Ivanov, D.A., Kustatscher, E.,

744 Leroy, S.A.G., McElwain, J.C., Opluštil, S., Popa, M.E., Seyfullah, L.J., Stolle,
745 E., Thomas, B.A., and Uhl, D., 2021, Plant diversity in deep time: 1. How well
746 can we identify past plant diversity in the fossil record? Palaeogeography,
747 Palaeoecology, Palaeoclimatology, v. 576, p. 110481.
748 Dal Corso, J., Song, H.J., Callegaro, S., Chu, D.L., Sun, Y.D., Hilton, J., Grasby, S.E.,
749 Joachimski, M.M., Wignall, P.B. 2022. Environmental crises at the Permian–
750 Triassic mass extinction. Nature Reviews Earth and Environment, v. 3, p. 197–
751 214. https://doi.org/10.1038/s43017-021-00259-4
752 Davydov, V.I., Karasev, E.V., Nurgalieva, N.G., Schmitz, M.D., Budnikov, I.V.,
753 Biakov, A.S., Kuzina, D.M., Silantiev, V.V., Urazaeva, M.N., Zharinova, V.V.
754 and Zorina, S.O., 2021, Climate and biotic evolution during the Permian-Triassic
755 transition in the temperate Northern Hemisphere, Kuznetsk Basin, Siberia,
756 Russia. Palaeogeography, Palaeoclimatology, Palaeoecology, v. 573, p. 110432.
757 Davydov, V.I. and Karasev, E.V., 2021, The Influence of the Permian-Triassic
758 Magmatism in the Tunguska Basin, Siberia on the Regional Floristic Biota of the
759 Permian-Triassic Transition in the Region. Frontiers in Earth Science, v. 9, p.
760 134.
761 DiMichele, W.A., Kerp, H., Tabor, N.J., and Looy, C.V., 2008, The so-called
762 “Paleophytic–Mesophytic” transition in equatorial Pangea — Multiple biomes
763 and vegetational tracking of climate change through geological time.
764 Palaeogeography, Palaeoclimatology, Palaeoecology, v. 268, p. 152–163.
765 DiMichele, W.A., Bashforth, A.R., Falcon-Lang, H.J. and Lucas, S.G., 2020.
766 Uplands, lowlands, and climate: Taphonomic megabiases and the apparent rise of
767 a xeromorphic, drought-tolerant flora during the Pennsylvanian-Permian

768 transition. Palaeogeography, Palaeoclimatology, Palaeoecology, v. 559, art.
769 109965.
770 Feng, Z., Wei, H.-B., Guo, Y., He, X.Y., Sui, Q., Zhou, Y., Liu, H.Y., Gou, X.D., and
771 Lü, Y., 2020, From rainforest to herbland: new insights into land plant responses
772 to the end–Permian mass extinction, Earth–Science Reviews, v. 204, p. 103153.
773 Fielding, C.R., Frank T.D., McLoughlin, S., Vajda, V., Mays, C., Tevyaw, A.P.,
774 Winguth, A., Winguth, C., Nicoll, R.S., Bocking, M., and Crowley, J.L., 2019,
775 Age and pattern of the southern high–latitude continental end–Permian extinction
776 constrained by multiproxy analysis. Nature Communications, v. 10, p. 385.
777 Foster, C.B., and Afonin, S.A., 2005, Abnormal pollen grains: an outcome of
778 deteriorating atmospheric conditions around the Permian–Triassic boundary.
779 Journal of the Geological Society, London, v. 162, p. 653–659.
780 Frank, T.D., Fielding, C.R., Winguth, A.M.E., Savatic, K., Tevyaw, A., Winguth, C.,
781 McLoughlin, S., Vajda, V., Mays, C., Nicoll, R. and Bocking, M., 2021. Pace,
782 magnitude, and nature of terrestrial climate change through the end-Permian
783 extinction in southeastern Gondwana. Geology, v. 49, p.1089–1095.
784 Gall, J. –C., and Grauvogel–Stamm, L., 2005, The early Middle Triassic 'Grès à
785 *Voltzia*' Formation of eastern France: a model of environmental refugium.
786 Comptes Rendus Palevol, v. 4, p. 637–652.
787 Gastaldo, R.A., Kamo, S.L., Neveling, J., Geissman, J.W., Looy, C.V., and Martini,
788 A.M., 2020, The base of the *Lystrosaurus* Assemblage Zone, Karoo Basin,
789 predates the end-Permian marine extinction: Nature Communications, v. 11, art.
790 1428.

791 Gothan, W., 1912, Paläobotanik. In: Korschelt, E., Linck, G., Schaum, K., Simon, H.
792 Th., Verworn, M., Teichmann, E. (Eds.), Handwörterbuch der
793 Naturwissenschaften. Gustav Fischer Verlag, Jena, pp. 408–460 (in German).
794 Guo, W.W., Tong, J.N., Tian, L., Chu, D.L., Bottjer, D.J., Shu, W.C., and Ji, K.X.,
795 2019, Secular variations of ichnofossils from the terrestrial Late Permian–Middle
796 Triassic succession in the Shichuanhe section in Shaanxi Province, North China.
797 Global and Planetary Change, v. 181, p. 102978.
798 Guo, W., Tong, J., He, Q., Hounslow, M.W., Song, H., Dal Corso, J., Wignall, P.B.,
799 Ramezani, J., Tian, L. and Chu, D., 2022. Late Permian–Middle Triassic
800 magnetostratigraphy in North China and its implications for terrestrial-marine
801 correlations. Earth and Planetary Science Letters, v. 585, art. 117519.
802 Guo, W., 2022. Late Permian–Middle Triassic magnetostratigraphic timescale from
803 terrestrial North China and secular variations of ichnofossils. PhD thesis, China
804 University of Geosciences, Wuhan, pp. 228.
805 Hilton, J., and Cleal, C.J., 2007, The relationship between Euramerican and
806 Cathaysian tropical floras in the Late Palaeozoic: palaeobiogeographical and
807 palaeogeographical implications. Earth–Science Reviews, v. 85, p. 85–116.
808 Hochuli, P.A., Sanson-Barrera, A., Schneebeli-Hermann, E. and Bucher, H., 2016.
809 Severest crisis overlooked—Worst disruption of terrestrial environments
810 postdates the Permian–Triassic mass extinction. Scientific Reports, v. 6, art.
811 28372.
812 Hochuli, P.A., Schneebeli–Hermann, E., Mangerud, G., and Bucher, H., 2017,
813 Evidence for atmospheric pollution across the Permian–Triassic transition.
814 Geology, v. 45, p. 1123–1126.

815 Hou, J.P. and S. Ouyang, 2000, Palynoflora from the Sunjiagou Formation in Liulin
816 County, Shanxi Province. Acta Palaeontologica Sinica, v. 39, p. 356–368.
817 Hu, B., Yang, W.T., Song, H.B., Wang, M., and Zhong, M.Y., 2009, Trace fossils and
818 ichnofabrics in the Heshanggou Formation of lacustrine deposits, Jiyuan Area,
819 Henan Province. Acta Sedimentologica Sinica, v. 27, p. 573–582 (in Chinese).
820 Ji, K.X., Wignall, P.B., Peakall, J., Tong, J.N., Chu, D.L., and Pruss, S.B., 2021,
821 Unusual intraclast conglomerates in a stormy, hot-house lake: the Early Triassic
822 North China Basin. Sedimentology, v.68, p. 3385–3404.
823 Ji, K.X., Wignall, P.B., Tong, J.N., Yu, Y.Y., Guo, W.W., Shu, W.C., and Chu, D.L.,
824 2022. Sedimentology of the latest Permian to Early Triassic in the terrestrial
825 settings of the North China Basin: Low-latitude climate change during a
826 warming-driven crisis. GSA Bulletin, https://doi.org/10.1130/B36260.1.
827 Jones, T.P., and Rowe, N.P., 1999, Fossil plants and spores: modern techniques.
828 Geological Society of London, pp. 420.
829 Kerp, H., 1990, The study of fossil gymnosperms by means of cuticular analysis.
830 Palaios, v. 5, 548–569.
831 Koll, R.A. and DiMichele, W.A., 2021. Dominance-diversity architecture of a mixed
832 hygromorphic-to-xeromorphic flora from a botanically rich locality in western
833 equatorial Pangea (lower Permian Emily Irish site, Texas, USA.
834 Palaeogeography, Palaeoclimatology, Palaeoecology, v. 563, art. 110132.
835 Kustatscher, E., Van Konijnenburg-Van Cittert, J.H.A., Bauer, K., Butzmann, R.,
836 Meller, B., and Fischer, T.C., 2012, A new flora from the Upper Permian of
837 Bletterbach (Dolomites, N–Italy). Review of Palaeobotany and Palynology, v.
838 182, p. 1–13.

839 Kustatscher, E., Bernardi, M., Petti, F.M., Franz, M., Van Konijnenburg-Van Cittert,
840 J.H.A., and Kerp, H., 2017, Sea-level changes in the Lopingian (late Permian) of
841 the northwestern Tethys and their effects on the terrestrial palaeoenvironments,
842 biota and fossil preservation. Global and Planetary Change, v. 148, p. 166–180.
843 Lee, M.S.Y., 1997, A taxonomic revision of pareiasaurian reptiles: implications for
844 Permian terrestrial palaeoecology. Modern Geology, v. 21, p. 231–298.
845 Liu, J., 2018, New progress on the correlation of Chinese terrestrial Permo-Triassic
846 strata. Vertebrata Palasiatica, v. 56, p. 327–342.
847 Liu, J., and Bever, G.S., 2018, The tetrapod fauna of the Upper Permian Naobaogou
848 Formation of China: A new species of *Elginia* (Parareptilia, Pareiasauria). Papers
849 in Palaeontology, v. 4, p. 197–209.
850 Liu, J., Xu, L., Jia, S.H., Pu, H.Y., and Liu, X.L., 2014, The Jiyuan tetrapod fauna of
851 the Upper Permian of China—2. stratigraphy, taxonomical review, and
852 correlation. Vertebrata Palasiatica, v. 52, p. 328–339.
853 Liu, J., and Sullivan, C., 2017, New discoveries from the *Sinokannemeyeria–*
854 *Shansisuchus* Assemblage Zone: 3. Archosauriformes from Linxian, Shanxi,
855 China. Vertebrata PalAsiatica, v. 55, p. 110–128.
856 Liu, J., Ramezani, J., Li, L., Shang, Q.H., Xu, G.H., Wang, Y.Y., and Yang, J.S.,
857 2018, High-precision temporal calibration of Middle Triassic vertebrate
858 biostratigraphy: U-Pb zircon constraints for the *Sinokannemeyeria* Fauna and
859 *Yonghesuchus*. Vertebrata PalAsiatica, v. 56, p. 16–24.
860 Liu, Y.Q., Kuang, H.W., Peng, N., Xu, H., Zhang, P., Wang, N.S., and An, W., 2015,
861 Mesozoic basins and associated palaeogeographic evolution in North China.
862 Journal of Palaeogeography, v. 4, p. 189–202.

Looy, C.V., Brugman, W.A., Dilcher, D.L., and Visscher, H., 1999, The delayed resurgence of equatorial forests after the Permian–Triassic ecologic crisis. Proceedings of the National Academy of Sciences, USA, v. 96, p. 13857–13862.

Looy, C.V., Twitchett, R.J., Dilcher, D.L., Van Konijnenburg-Van Cittert, J.H.A., and Visscher, H., 2001, Life in the end-Permian dead zone. Proceedings of the National Academy of Sciences, USA, v. 98, p. 7879–7883.

Lu, J., Zhang, P.X., Yang, M.F., Shao, Y.L., and Hilton, J., 2020, Continental records of organic carbon isotopic composition ($\delta^{13}C_{org}$), weathering, paleoclimate and wildfire linked to the End–Permian mass extinction, Chemical Geology, v. 558, p. 119764.

Mays, C., Vajda, V., Frank, T., Fielding, C., Nicoll, R.S., Tevyaw, A., and McLoughlin, S., 2020. Refined Permian-Triassic floristic timeline reveals early collapse and delayed recovery of south polar terrestrial ecosystems. GSA Bulletin, v. 132, p. 1489–1513.

Mays, C., McLoughlin, S., Frank, T.D., Fielding, C.R., Slater, S.M. and Vajda, V., 2021a. Lethal microbial blooms delayed freshwater ecosystem recovery following the end-Permian extinction. Nature communications, v. 12, p. 1–11.

Mays, C., Vajda, V. and McLoughlin, S., 2021b. Permian–Triassic non-marine algae of Gondwana—distributions, natural affinities and ecological implications. Earth-Science Reviews, v. 212, art. s103382.

McLoughlin, S., 2001, The breakup history of Gondwana and its impact on pre-Cenozoic floristic provincialism. Australian Journal of Botany, v. 49, p. 271–300.

McLoughlin, S., 2011, *Glossopteris*—insights into the architecture and relationships of an iconic Permian Gondwanan plant. Journal of the Botanical Society of Bengal, v. 65, p. 1–14.

888 McLoughlin, S., Nicoll, R.S., Crowley, J.L., Vajda, V., Mays, C., Fielding, C.R.,
889 Frank, T.D., Wheeler, A. and Bocking, M., 2021. Age and paleoenvironmental
890 significance of the Frazer Beach Member—a new lithostratigraphic unit
891 overlying the end-Permian extinction horizon in the Sydney Basin, Australia.
892 Frontiers in Earth Science, v. 8, art. 600976.
893 Nesbitt, S.J., J. Liu and C. Li, 2011. A sail-backed suchian from the Heshanggou
894 Formation (Early Triassic: Olenekian) of China. Earth and Environmental
895 Science Transactions of the Royal Society of Edinburgh, v. 101, p. 271–284.
896 Niklas, K.J., Tiffney, B.H., and Knoll, A.H., 1983, Patterns in vascular land plant
897 diversification. Nature, v. 303, p. 614–616.
898 Nowak, H., Schneebeli-Hermann, E. and Kustatscher, E., 2019. No mass extinction
899 for land plants at the Permian–Triassic transition. Nature communications, v. 10,
900 p. 384.
901 Ouyang, S., and Norris, G., 1988, Spores and pollen from the Lower Triassic
902 Heshanggou Formation, Shaanxi Province, North China. Review of Palaeobotany
903 and Palynology, v. 54, p. 187–231.
904 Ouyang, S., and Wang, R.N., 1985, Age assignment of the Pingdingshan Member in
905 Henan and Anhui provinces. Experimental Petroleum Geology, v. 7, p. 141–147.
906 Ouyang, S., and Zhang, Z.L., 1982, Early Triassic palynological assemblage in
907 Dengfeng, Northwestern Henan. Acta Palaeontologica Sinica, v. 21, p. 685–696.
908 Pang, Q.Q.,1989, The Early–Middle Triassic stratigraphy and Ostracoda from the
909 Yima area in Henan province. Journal of Hebei College of Geology, v. 12, p.
910 325–345.
911 Qu, L.F., 1980, Triassic spore and pollen fossils. In: Institute of Geology, Chinese
912 Academy of Geological Sciences, Mesozoic stratigraphy and paleontology of the

913 Shaanxi-Gansu-Ningxia Basin. Vol. 1. Publishing House of Geology, Beijing,
914 China, p. 115–143.
915 Qu, L.F., 1982, The palynological assemblage from the Liujiagou Formation of
916 Jiaocheng, Shanxi. Bulletin of Geological Institute, Chinese Academy of
917 Geological Society, v. 4, p. 83–93.
918 Qu, L.F., Yang, J.D., Bai, Y.H., and Zhang, Z.L., 1983. A preliminary discussion on
919 the characteristics and stratigraphic divisions of Triassic spores and pollen in
920 China. Bulletin Chinese Academy of Geological Sciences, v. 5, p. 81–94.
921 Rees, P.M., 2002, Land-plant diversity and the end-Permian mass extinction.
922 Geology, v. 30, p.827–830.
923 Retallack, G.J., and Krull, E.S., 1999, Landscape ecological shift at the Permian-
924 Triassic boundary in Antarctica. Australian Journal of Earth Sciences, v. 46, p.
925 785–812.
926 Retallack, G.J., Veevers, J.J., and Morante, R., 1996, Global coal gap between
927 Permian-Triassic extinction and Middle Triassic recovery of peat–forming plants.
928 Geological Society of America Bulletin, v. 108, p. 195–207.
929 Scotese, C.R., 2021. An Atlas of Phanerozoic Paleogeographic Maps: The seas come
930 in and the seas go out. Annual Review of Earth and Planetary Sciences, v. 49, p
931 679–728.
932 Sephton, M.A., Jiao, D., Engel, M.H., Looy, C.V., and Visscher, H., 2015, Terrestrial
933 acidification during the end-Permian biosphere crisis? Geology, v. 43, p. 159–
934 162.
935 Sepkoski J. J. Jr., 1984, Kinetic model of Phanerozoic taxonomic diversity. III. Post–
936 Paleozoic families and mass extinctions. Paleobiology, v. 10, p. 246–267.

937 Shen, W.J., Sun, Y.G., Lin, Y.T., Liu, D.H., and Chai, P.X., 2011, Evidence for
938 wildfire in the Meishan section and implications for Permian–Triassic events.
939 Geochimica et Cosmochimica Acta, v. 75, p. 1992–2006.
940 Shu, W.C., Tong, J.N., Tian, L., Benton, M.J., Chu, D.L., Yu, J.X., and Guo, W.W.,
941 2018, Limuloid trackways from Permian-Triassic continental successions of
942 North China. Palaeogeography, Palaeoclimatology, Palaeoecology, v. 508, p. 71–
943 90.
944 Song, H.J., Wignall, P.B., Tong, J.N., Song, H.Y., Chen, J., Chu, D.L., Tian, L., Luo,
945 M., Zong, K.Q., Chen, Y.L., Lai, X.L., Zhang, K.X., and Wang, H.M., 2015,
946 Integrated Sr isotope variations and global environmental changes through the
947 Late Permian to early Late Triassic. Earth and Planetary Science Letters, v. 424,
948 p. 140–147.
949 Stanley, S.M., 2016. Estimates of the magnitudes of major marine mass extinctions in
950 earth history. Proceedings of the National Academy of Sciences, v. 113, p.
951 E6325–E6334.
952 Stevens, L.G., Hilton, J., Bond, D.P.G., Glasspool, I.J., and Jardine, P.E., 2011,
953 Radiation and extinction patterns in Permian floras from North China as
954 indicators for environmental and climate change. Journal of the Geological
955 Society, London, v. 168, p. 607–619.
956 Sun, Y.D., Joachimski, M.M., Wignall, P.B., Yan, C.B., Chen, Y.L., Jiang, H.S.,
957 Wang, L.N., and Lai, X.L., 2012, Lethally hot temperatures during the Early
958 Triassic Greenhouse. Science, v. 338, p. 366–370.
959 Tong, J.N., Chu, D.L., Liang, L., Shu, W.C., Song, H.J., Song, T., Song, H.Y., and
960 Wu, Y.Y., 2018, Triassic integrative stratigraphy and timescale of China. Science
961 China Earth Sciences, v. 62, p. 189–222.

962 Tu, C.Y., Chen, Z.Q., Retallack, G.J., Huang, Y.G., and Fang,Y.H., 2016,
963 Proliferation of MISS–related microbial mats following the end-Permian mass
964 extinction in terrestrial ecosystems: Evidence from the Lower Triassic of the
965 Yiyang area, Henan Province, North China. Sedimentary Geology, v. 333, p. 50–
966 69.
967 Vajda, V., McLoughlin, S., Mays, C., Frank, T.D., Fielding, C.R., Tevyaw, A.,
968 Lehsten, V., Bocking, M., and Nicoll, R.S., 2020, End-Permian (252 Mya)
969 deforestation, wildfires and flooding—An ancient biotic crisis with lessons for
970 the present. Earth and Planetary Science Letters, v. 529, p. 115875.
971 Visscher, H., Looy, C.V., Collinson, M.E., Brinkhuis, H., van Konijnenburg-van
972 Cittert, J.H.A., Kürschner, W.M., and Sephton, M.A., 2004, Environmental
973 mutagenesis during the end-Permian ecological crisis. Proceedings of the
974 National Academy of Sciences, USA, v. 101, p. 12952–12956.
975 Wang, J., 2010. Late Paleozoic macrofloral assemblages from Weibei Coalfield, with
976 reference to vegetational change through the Late Paleozoic Ice-age in the North
977 China Block. International Journal of Coal Geology, v. 83, p. 292–317.
978 Wang, J., Liu, H.Q., Shen, G.L., and Zhang, H., 1998, Notes on the island distribution
979 pattern of the Permian Cathaysian flora in China: an example of the application
980 of the equilibrium theory of island biogeography in palaeobiogeography.
981 Palaeogeography Palaeoclimatology Palaeoecology, v. 142, p. 23–31.
982 Wang, J.Y., Yi, J., Liu, J., 2019, The first complete pareiasaur skull from China. Acta
983 Palaeontologica Sinica, v. 58, p. 216–221.
984 Wang, L.X., 1983. Triassic of Shanxi. Shanxi Provincial Geological Prospecting
985 Bureau, 198 pp.

Wang, L.X., Xie, Z.M., and Wang, Z.Q., 1978, On the occurrence of *Pleuromeia* from the Qinshui basin in Shanxi province. Acta Palaeontologica Sinica, v. 17, p. 195–211.

Wang R.N., 1981, The "Shichienfeng Formation" of Yongcheng, Henan province and other adjacent area. Journal of Stratigraphy, v. 5, p. 180–189.

Wang, Z.Q., 1993, Evolutionary ecosystem of Permian–Triassic redbeds in North China: a historical record of global desertification. New Mexico Museum of Natural History and Science Bulletin, v. 3, p. 471–476.

Wang, Z.Q., 1996, Recovery of vegetation from the terminal Permian mass extinction in North China. Review of Palaeobotany and Palynology, v. 91, p. 121–142.

Wang, Z.Q., and Wang, L.X., 1982, A new species of the lycopsid *Pleuromeia* from the early Triassic of Shanxi, China and its ecology. Palaeontology, v. 25, p. 215–225.

Wang, Z.Q., and Wang, L.X., 1986, Late Permian fossil plants from the lower part of the Shiqianfeng (Shihchienfeng) group in North China. Bulletin Tianjin Institute of Geology and Mineral Resources, v. 15, p. 1–120.

Wignall, P.B., 2015, The worst of times. Princeton University Press, p. 64–75.

Wu, Q., Ramezani, J., Zhang, H., Wang, J., Zeng, F.G., Zhang, Y.C., Liu, F., Chen, J., Cai, Y.F., Hou, Z.S., Liu, C., Yang, W., Henderson, C.M. and Shen, S.Z., 2021, High-precision U-Pb age constraints on the Permian floral turnovers, paleoclimate change, and tectonics of the North China block. Geology, v. 49, p. 677–681.

Wu, Y.Y., Tong, J.N., Algeo, T.J., Chu, D.L., Cui, Y., Song, H.Y., Shu, W.C., and Du, Y., 2020, Organic carbon isotopes in terrestrial Permian-Triassic boundary

1010 sections of North China: Implications for global carbon cycle perturbations.
1011 Geological Society of America Bulletin, v. 132, p. 1106–1118.
1012 Xiong, C.H., and Wang, Q., 2011, Permian–Triassic land-plant diversity in South
1013 China: Was there a mass extinction at the Permian/Triassic boundary?
1014 Paleobiology, v. 37, p. 157–167.
1015 Xu, L., Li, X.W., Jia, S.H. and Liu, J., 2015, The Jiyuan tetrapod Fauna of the Upper
1016 Permian of China: New pareiasaur material and the reestablishment of *Honania*
1017 *complicidentata*. Acta Palaeontologica Polonica, v. 60, p.689–700.
1018 Xu, Z., Hilton, J., Yu. J.X., Wignall, P.B., Yin, H.F., Xue, Q., Ran, W.J., Hui, L.,
1019 Shen, J., and Meng, F.S., 2022. Mid-Permian to Late Triassic plant species
1020 richness and abundance patterns in South China: Co-evolution of plants and the
1021 environment through the Permian-Triassic transition. Earth-Science Reviews.
1022 https://doi.org/10.1016/j.earscirev.2022.104136
1023 Yang, G.X., and Wang, H.S., 2012, Yuzhou Flora- A hidden gem of the Middle and
1024 Late Cathaysian Flora. Science China Earth Sciences, v. 55, p. 1601–1619.
1025 Yin, H.F., and Lin, H.M., 1979, Marine Triassic faunas and the geologic time from
1026 Shihchienfeng Group in the northern Weihe River Basin, Shaanxi Province. Acta
1027 Stratigraphica Sinica, v. 3, p. 233–241 (in Chinese).
1028 Yu, J.X., Broutin, J., Chen, Z.Q., Shi, X., Li, H., Chu, D.L., and Huang, Q.S., 2015,
1029 Vegetation changeover across the Permian–Triassic Boundary in Southwest
1030 China: extinction, survival, recovery and palaeoclimate: A critical review. Earth-
1031 Science Reviews, v. 149, p. 203–224.
1032 Yu, Y.Y., Tian, L., Chu, D.L., Song, H.Y., Guo, W.W. and Tong, J.N., 2022, Latest
1033 Permian–Early Triassic paleoclimatic reconstruction by sedimentary and isotopic

analyses of paleosols from the Shichuanhe section in central North China Basin. Palaeogeography, Palaeoclimatology, Palaeoecology, v. 585, p.110726.

Zheng, D., Chang, S.C., Wang, H., Fang, Y., Wang, J., Feng, C., Xie, G., Jarzembowski, E.A., Zhang, H., and Wang, B., 2018, Middle-Late Triassic insect radiation revealed by diverse fossils and isotopic ages from China. Science advances, v. 4, p. eaat1380.

Zhu, R.K., Xu, H.X., Deng, S.H., and Guo, H.L., 2007, Lithofacies palaeogeography of the Permian in northern China. Journal of Palaeogeography, v. 9, p. 133–142.

Zhu, Z.C., Kuang, H., Liu, Y.Q., Benton, M.J., Newell, A.J., Xu, H., An, W., Ji, S.A., Xu, S.C., Peng, N., and Zhai, Q.G., 2020, Intensifying aeolian activity following the end-Permian mass extinction: evidence from the Late Permian–Early Triassic terrestrial sedimentary record of the Ordos Basin, North China. Sedimentology, v. 67, p. 2691–2720.

FIGURES AND TABLES CAPTIONS

Figure 1. (A) Late Permian paleophytogeographical maps and distribution of typical Early Triassic fossil plant taxa during the Late Permian to Early Triassic (Broutin et al. 1995; McLoughlin 2001, 2011); base map adapted from Scotese (2021). (B) Paleogeographic map of the Late Permian and main sections of this study in North China; base map modified from Zhu et al. (2007). (C) Palaeogeographic map of the Early Triassic and main sections of this study in North China; base map modified from Liu et al. (2015). (D) Geographic distributions of fossil plant locations from the Sunjiagou (SJG), Liujiagou (LJG), Heshanggou (HSG) and Ermaying (EMY) formations in North China (Supplementary Data File 1).

Figure 2. Lithological columns of the studied sections showing the lithology and the position of the fossil horizons and some special sedimentary structures. Lower dotted line marks the end-Permian Plant Extinction event (EPPE), the gray area indicates the ecological disturbance interval without fossil plants, and the upper dashed line marks the occurrence of Early Triassic fossil plants in the studied sections. Abbreviation: Fm., Formation, Tetra., Tetrapods.

Figure 3. Plant fossils, cuticles and *in situ* pollens from the top part of the Upper Shihhotse Formation of the Shichuanhe and Liulin sections. A–C, *Autunia*–type ovuliferous organs. D, small fragmentary pinna of *Sphenopteris*. E, F, strap-like leaf in E and broken leaf in F of *Taeniopteris* with simple parallel lateral veins arising from the midvein at an angle of nearly 90°. G–J, broken leaves of ginkgophytes, G and H, broken leaves of ginkgophyte type 2 with horn-like shape and dichotomous-patterned veins, I and J, broken wedged-shape leaves with the bifurcated rounded apex of ginkgophyte type 1 with strong petioles. K–O, T, W, shoots and cuticle of conifer type 2, K with possible terminate cone on the shoot, the cuticle in W is from the shoot in T. P, possible cone of a conifer. Q–S, U, V, X, Y, shoots, cuticles and *in situ* pollens of conifer type 0, U and V are cuticles macerated from the shoot in S, X and Y are *in situ* pollens "picked out" directly from the shoots in Q–S and pollen in Y was photographed under SEM. Scale bars: A–D, L, T are 5 mm. E–K, M–S are 1 cm. U, V, X, Y are 50 μm, W is 20 μm. A–D, F, I–J, K–O, P from the Shichuanhe section. E, G–H, Q–T, Q–Y from the Liulin section.

Figure 4. Plant fossils, cuticles and *in situ* pollens from the lower part of the Sunjiagou Formation of the Liulin, Dayulin and Zishiya sections. A, fragments of

pinnule of pteridophyte with dichotomous veins. B–I, M–O, vegetative terminal pinnae of *Germaropteris martinsii* and its cuticles, triangular arrows in N and O show the base of trichome, D before processing, E after processing, F–I and M–O are from the red rectangular area of E. J–L, fertile parts of the *Autunia*-type organ. P–Y, MM, shoots and isolated leaves of conifer type 3 of *Pseudovoltzia* with well-preserved cuticle, R–X are from Q, S–X is from the red rectangular area of R. AA, bract-scale complexes of fossil conifers. BB–CC, heterophyll shoot and its cuticles of conifer type 2. DD, EE, PP, SS, male cone of conifer and its *in situ* pollens (possible *Gardenasporites*), EE is a reconstruction of DD, PP is the distal view and SS is the proximal view of pollen grains. FF–GG, some shoots of conifer type 4. Z, HH–LL, NN, OO, QQ, RR, some conifer shoots with their cuticles of conifer type 1. Scale bars: A, J, Y, Z, AA, BB are 5 mm. K, L, DD–HH, KK, LL, MM are 1 cm. B–E, P–R are 1 mm. F–I, N–O, T–X, CC, NN–SS are 50 μm; M, S, II are 500 μm; JJ is 200 μm. A–J, M–O, DD–GG, PP, SS from the Liulin section. P–Z, AA–CC, HH–JJ, NN–OO, QQ, RR from the Dayulin section. K, L, KK–MM from the Zishiya section.

Figure 5. Strobili of *Pleuromeia* and pinnate fragments of pteridophylls from the upper part of the Liujiagou Formation at Peijiashan. A, B, pinnate fragments of *Scolopendrites*. C–K, strobili of *Pleuromeia*. F–K was processed under CT scanning. All scale bars are 1 cm.

Figure 6. *In situ* stems/rhizomorphs and dispersed megasporophylls of *Pleuromeia*, dispersed broken megasporophylls of *Tomiostrobus*, *in situ* rhizomes and dispersed stems of *Neocalamites* and *Equisetites* and isolated possible male cone, bract-scale complexes and seeds of voltzian conifers from the basal Heshanggou Formation of

Heshun. A–D, *in situ* stems/rhizomorphs of *Pleuromeia*, C is the bottom of B showing four-lobed rhizomorphs. E–J, some *in situ* rhizomes and dispersed stems of *Neocalamites*, F, triangular arrow shows the linear whorled leaves at the node; H, triangular arrow shows one small branch base at the node; J, shows the underground part of the rhizome and triangular arrow shows the upright stem. K shows broken stem of *Equisetites*. L, dispersed broken megasporophyll with a long tip characteristic of *Tomiostrobus*. M, dispersed megasporophyll of *Pleuromeia*. N, one isolated possible male cone. O, bract-scale complexes and cordiform seeds of voltzian conifers. Scale bars: A, B, D, J are 5 cm; C is 2 cm; E–I, K–O are 1 cm.

Figure 7. Plants from the Lower Heshanggou Formation of Yushe. A–D, megasporophylls of *Pleuromeia*, some microconchids on the surface of D at the triangular arrow. E, F, pinnae of *Anomopteris*. G, stem of *Pleuromeia*. H, strobilus of *Pleuromeia*. I, the broken stem of *Neocalamites*. J–L, *in situ* rhizophores of *Pleuromeia*. M–O, leaves of *Tongchuanophyllum*, showing feeding holes on the surface and margins of O at the triangular arrow. P–Q, bract-scale complexes of voltzian conifers. Scale bars: A, C, F, Q are 5 mm; B, D, E, G–P are 1 cm.

Figure 8. Some plant fossils from the Ermaying Formation of Yushe. A–C, some rhizophores of *Pleuromeia*. D–F, some broken sphenophyte stems of probably *Neocalamites*, showing possible invertebrate burrows inside the cast of the stem F. G–I, some woody plant fossil wood casts. Scale bars: A–D are 1 cm; E–I are 5 cm.

Figure 9. Other fossils associated with fossil plants. A–D, CT scanned 3D photos of Temnospondyli tooth from fossil-plant-bearing horizon of the Upper Shihhotse

Formation in the Shichuanhe section showing well-preserved inner structure; E, fragment of insect wing fossil; F, many microconchids found on some plant remains; G, some ophiurids; H–K, M, R, some conchostracans (H–K, *Pseudestheria* spp.; M, *Euestheria gutta*; R, *Magniestheria mangaliensis*); L, some lingulids; N–Q, S, T, some bivalves (N, *Pteria ussurica variabilis*; O, *Wilkingia* sp.; P, *Modiolus* sp.; Q, *Leptochondria* sp.; S, *Palaeoneilo elliptica*; T, *Promyalina putiatinensis*). Scale bars: A–G, O, P, T is 1 cm; H–N, Q–S is 1 mm. E, F, L–N were found in the rich sporomorph horizon of the Sunjiagou Formation in the Shichuanhe section; G and R were found in rich sporomorph horizon of the Qishan Formation in the Zishiya section; H-K were found with fossil plants in the Lower Sunjiagou Formation, H–J, in the Liulin section; K, in the Dayulin section; O–Q, S, T were found in the fossil-plant-bearing horizon of the Sunjiagou Formation in the Zishiya section.

Figure 10. Range chart of floras from North China from the Cisuralian to Middle Triassic interval. Five floras, one of which includes two sub-floras, and five floral transitions including an extirpation event, two turnovers and two radiation events are recognized here (Supplementary Data File 2, 3). g. extinction, gigantopterid flora extirpation; T1–T5, floral transition 1–5; EPPE, end-Permian Plant Extinction event. References of the previous studies can be seen in Supplementary Data File 4. Plant zones or subzones or assemblages in previous studies (see Supplementary Data File 4): *CrSZ*, *PZ*, *UZ*, *PjSZ*, *PeSZ*, *PsSZ*, *TZ*, *ISZ*, *SSZ*, *GLF*, *GLP*, *UY*, *GMLF*, *MPL*, *PSP*, *UP*; floras in this study (see Supplementary Data File 4): Voltziales, the Voltziales flora; gw, the ginkgophyte–walchian Voltziales subflora; Voltz., the voltzian Voltziales subflora; *PN*, the *Pleuromeia–Neocalamites* flora; *PT* flora, the

Pleuromeia–Tongchuanophyllum flora; *LV* flora, the *Lepacyclotes–Voltzia* flora. Te., tectonism; Wu., Wuchiapingian.

Figure 11. Hierarchical clustering and *k*–means clustering for five floras and three main phases from Permian to Middle Triassic in North China. A. Hierarchical clustering–complete linkage analysis showing five different floras from Permian to Middle Triassic in North China; B. k–means clustering analysis showing three main phases from Lopingian to Middle Triassic in North China. a. the gigantopterid flora extirpation (T1) and the absence of the coal deposits, b. End-Permian Plant extinction (EPPE, T3), c. Gradual recovery of floras (T5). gigantopter. flora, the gigantopterid flora; Volt. flora, the Voltziales flora; *PN* flora, the *Pleuromeia–Neocalamites* flora; *PT* flora, the *Pleuromeia–Tongchuanophyllum* flora; *LV* flora, the *Lepacyclotes–Voltzia* flora. 1–5, cluster centroids; T1–T5, floral transition 1–5.

Figure 12. Model of floral community's changeovers associated with different animals during the Permian–Triassic crisis in North China. 1, *Tomiostrobus*/*Lepacyclotes*; 2. *Pleuromeia*; 3. *Sphenophytes*; 4, 19. Tree ferns; 5. Small Pteridophytes (e.g., *Anomopteris*/*Scolopendrites*); 6. Pteridosperms; 7. Cycads; 8. Ginkgophytes; 9. Conifers; 10. Ostracods; 11. Conchostracans; 12. Triopsidae; 13. Bivalves; 14. Insects; 15. Fishes; 16. MISS; 17. Lingulids; 18. *Yuania*; 20. gigantopterids; 21. Lepidodendrales. TED interval, the terrestrial ecological disturbance interval; LMUUSHZ, Lower–Middle–Upper Upper Shihhotse Formation; tUSHZ, topmost Upper Shihhotse Formation; Fm., Formation; g. extinction, gigantopterid flora extinction; T1–T5, floral transition 1–5; EPPE, end-Permian plant extinction event.

Figure 13. Late Permian to Triassic biotic and environmental changes in North China. Including diversity of plant, insect, tetrapod, fish, invertebrate and trace fossils associated with the environmental changes of coal deposits, red beds and humid/arid climates. Changes of coal deposits and red beds are modified from Wang (2010) and other data in Supplementary Data File 2–9. Fms, Formations; USHZ, the Upper Shihhotse Formation; SJG, the Sunjiagou Formation; LJG, the Liujiagou Formation; HSG, the Heshanggou Formation; EMY, the Ermaying Formation; Spo., Sporomorph assemblages; Cisura., Cisuralian; Loping., Lopingian; Wu.–Cha., Wuchiapingian–Changhsingian. TED interval is terrestrial ecological disturbance interval; gig. flora, the gigantopterid flora; Volt. flora, the Voltziales flora; *PN* flora, the *Pleuromeia–Neocalamites* flora; *PT* flora, the *Pleuromeia–Tongchuanophyllum* flora; *LV* flora, the *Lepacyclotes–Voltzia* flora. Sporomorph assemblages: *Patellisporites meishanensis* biozone (*Pm*); *Lueckisporites virkkiae–Jugasporites schaubergeroides* assemblage (*LvJs*); *Aratrisporites–Alisporites* assemblage (*AA*); *Densoisporites nejburgii–Lunatisporites–Cycadopites* assemblage (*DnLC*); *Cycadopites–Lunatisporites–Verrucosisporites* assemblage (*CLV*); *Punctatisporites–Chordasporites* (*PC*) assemblage see in Fig. S2; bioturbation intensity (The Bedding Plane Bioturbation Index (BPBI) and ichnofabric index (ii)) data from (Guo et al., 2019). Dashed lines mark position of two losses of diversity, the lowermost an extirpation event and the upper extinctions of the EPPC; three dotted lines mark position of three transitions the lowermost a turnover, the upper two radiations; gE, gigantopterid flora extirpation; T1–T5, floral transition 1–5; EPPE, end-Permian Plant Extinction event.

1207 Table 1. The number of specimens of macrofossil plants from different formations
1208 and sections in this study. USH Fm., Upper Shihhotse Formation; SJG Fm., Sunjiagou
1209 Formation; LJG Fm., Liujiagou Formation; HSG Fm., Heshanggou Formation; T.,
1210 total specimens.

	Liulin Section	Peijiashan Section	Dayulin Section	Shichuanhe Section	Zishiya Section	Heshun Section	Yushe Section	Pingyao Section	T.
HSG Fm.							280	120	400
LJG Fm.		80		10		10			100
SJG Fm.	206		37		202				445
USH Fm.	46			385					432
T.	252	80	37	395	202	10	280	120	1337

1211

1212

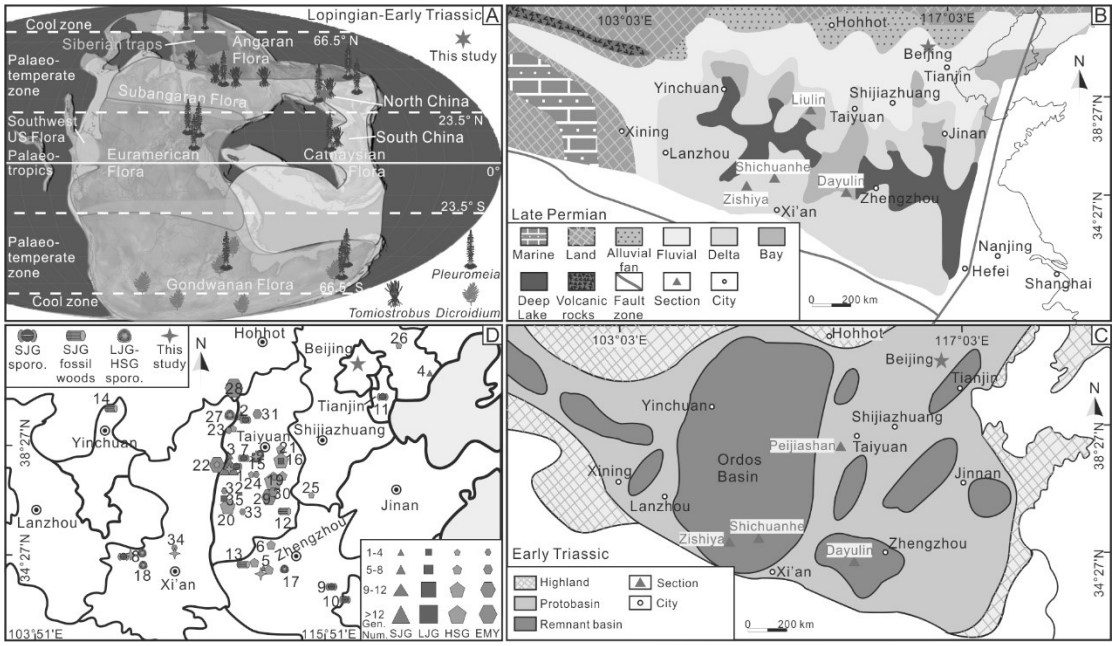

1213

1214 Figure 1

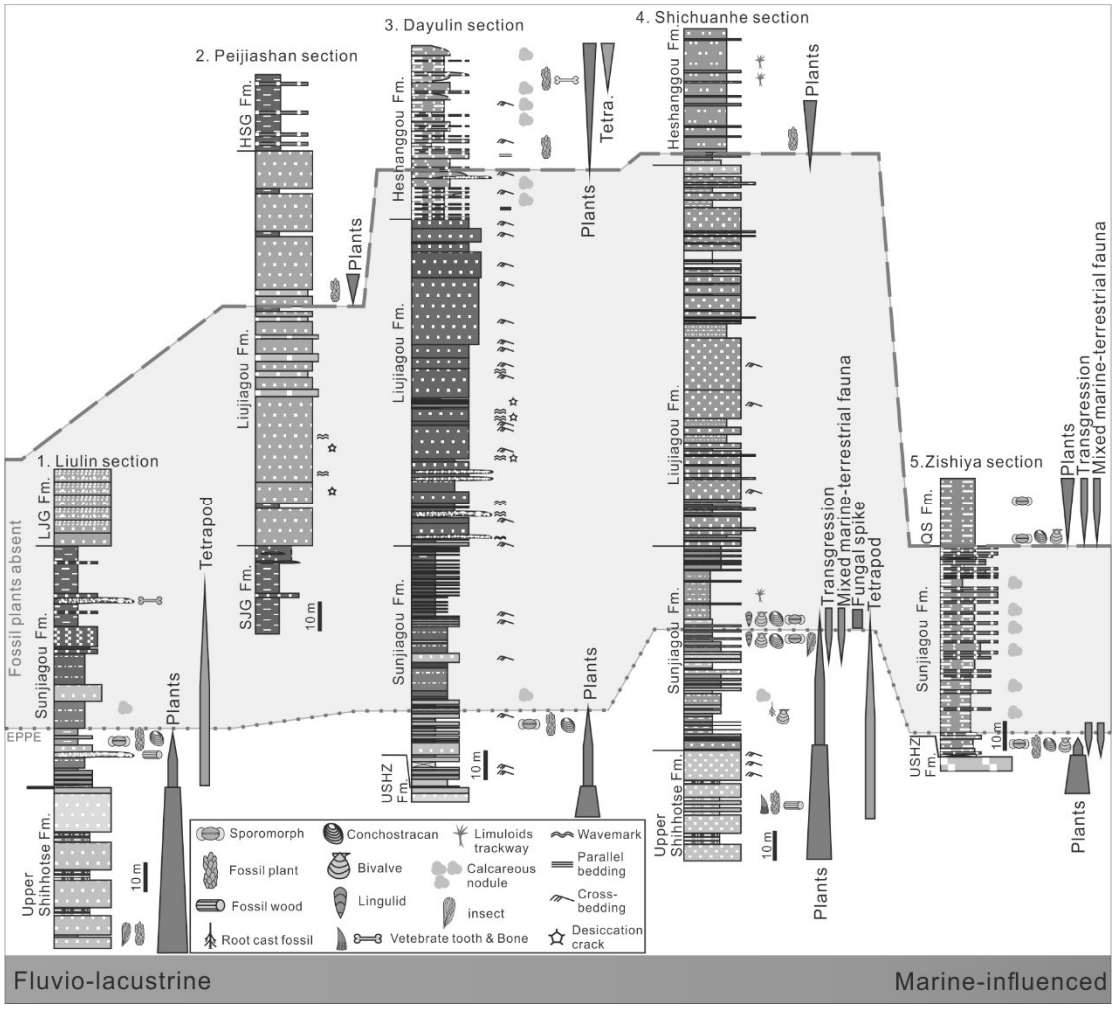

1215

1216 Figure 2

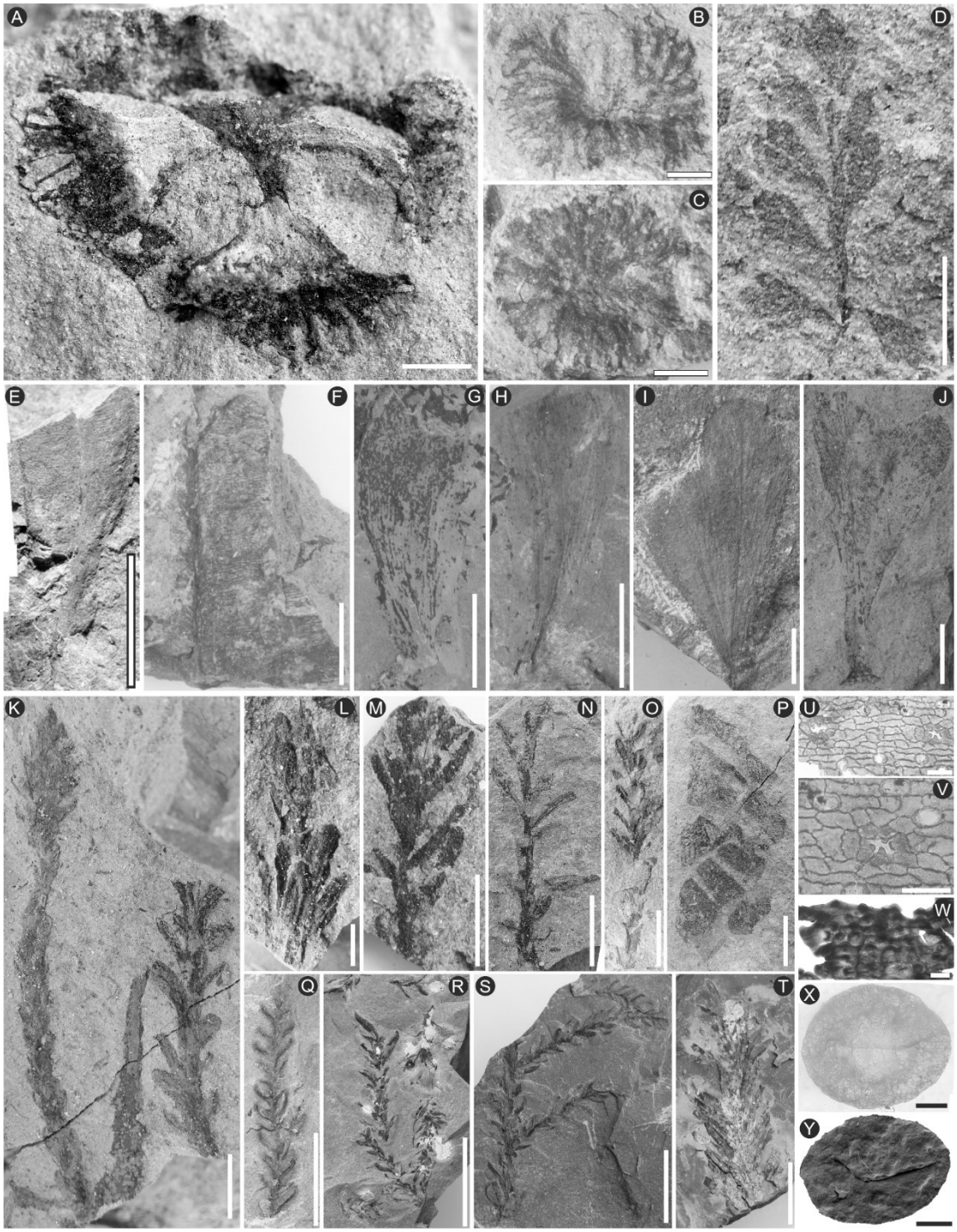

1217
1218 Figure 3

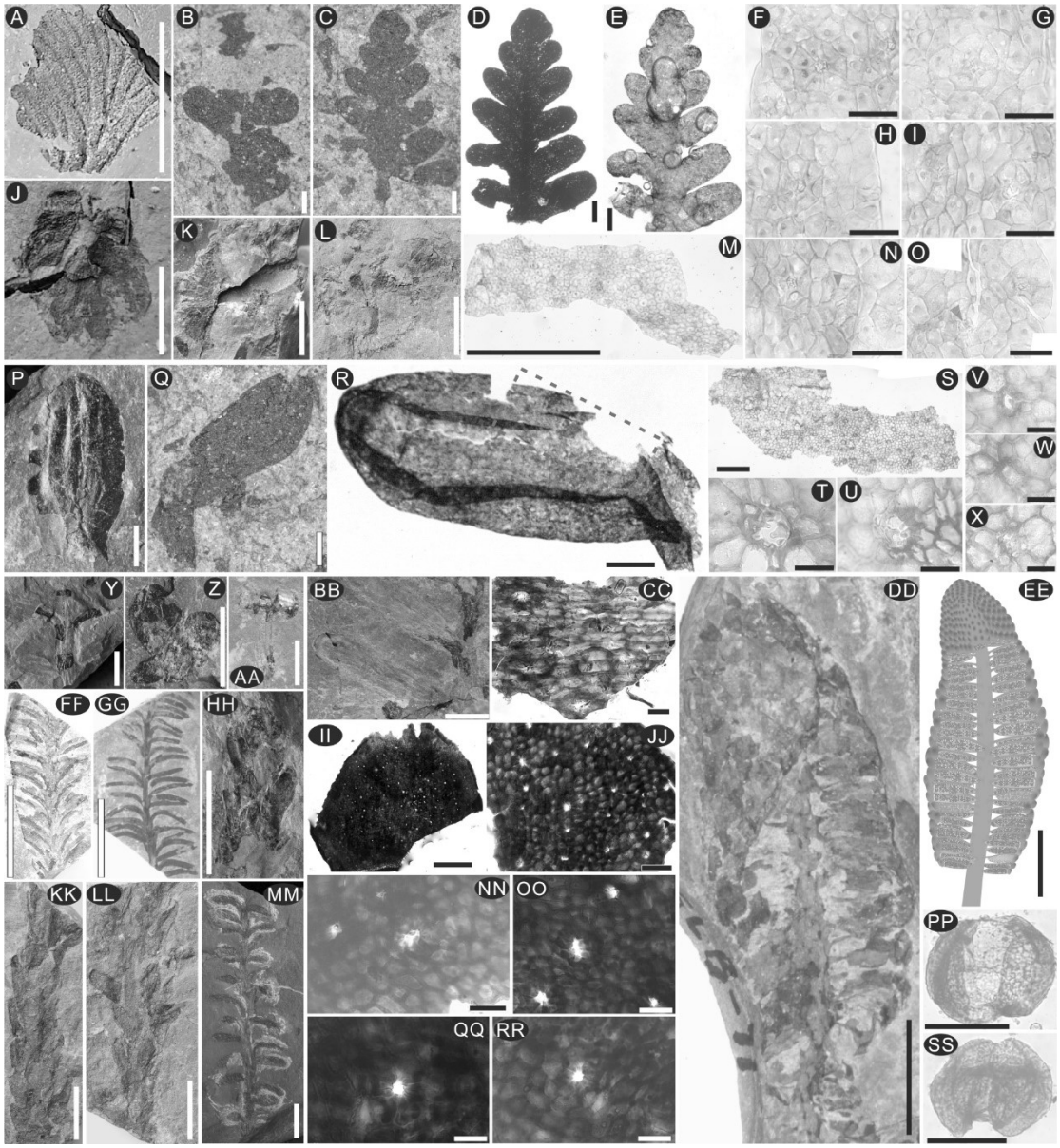

1219
1220 Figure 4

1221

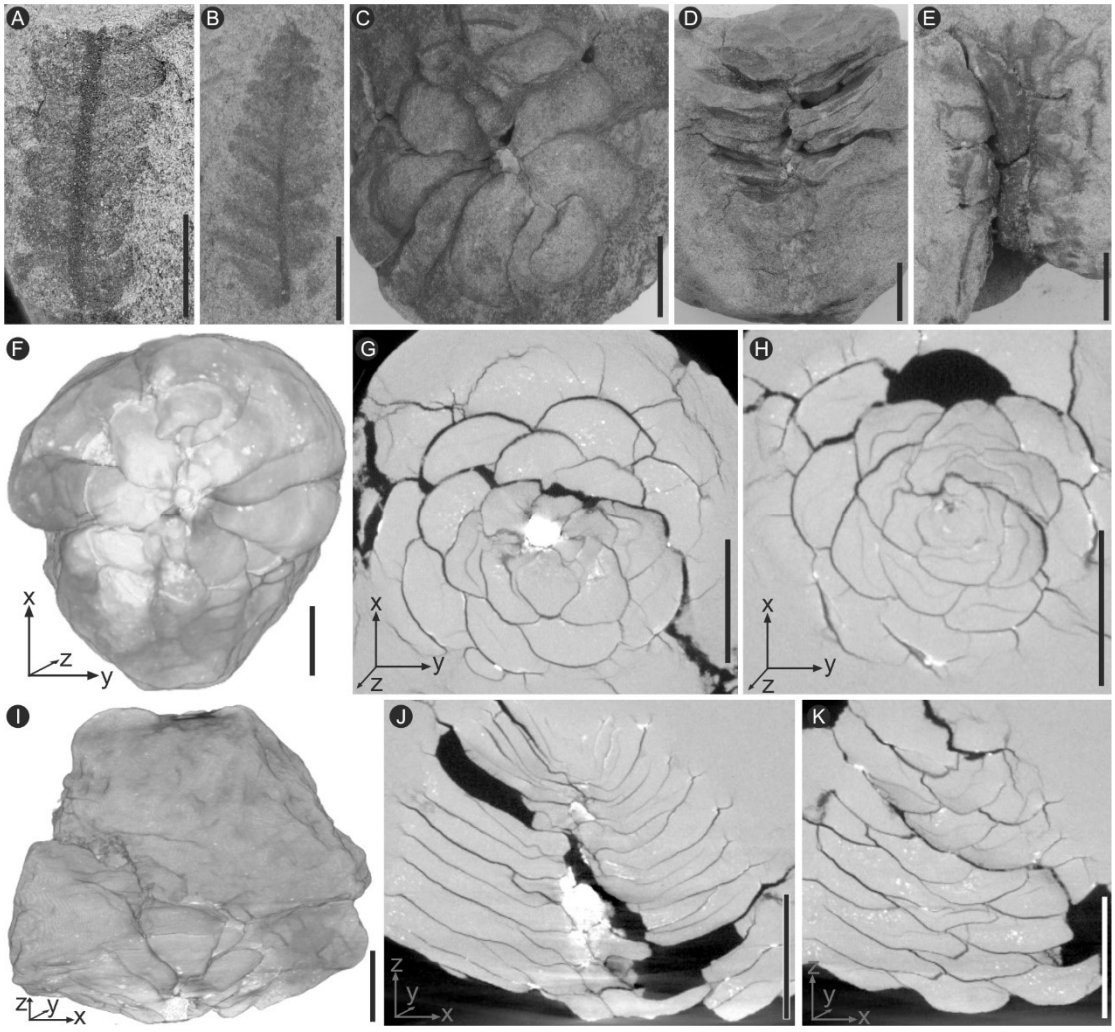

Figure 5

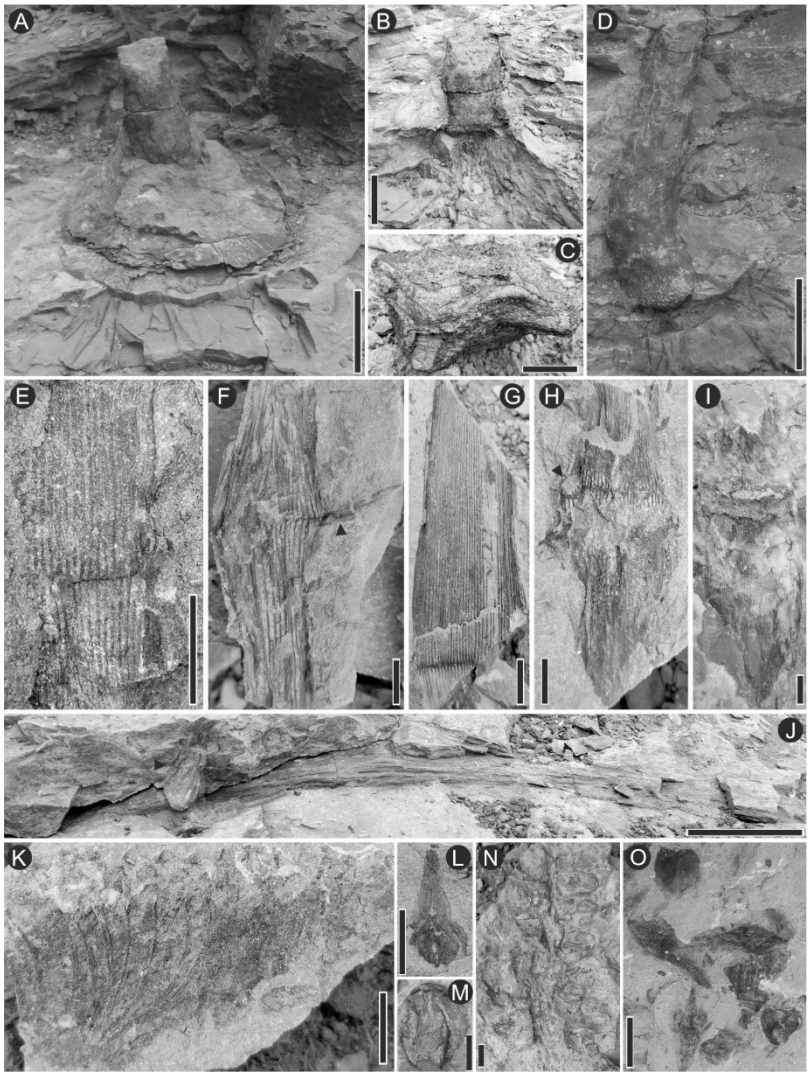

1225

1226 Figure 6

1227

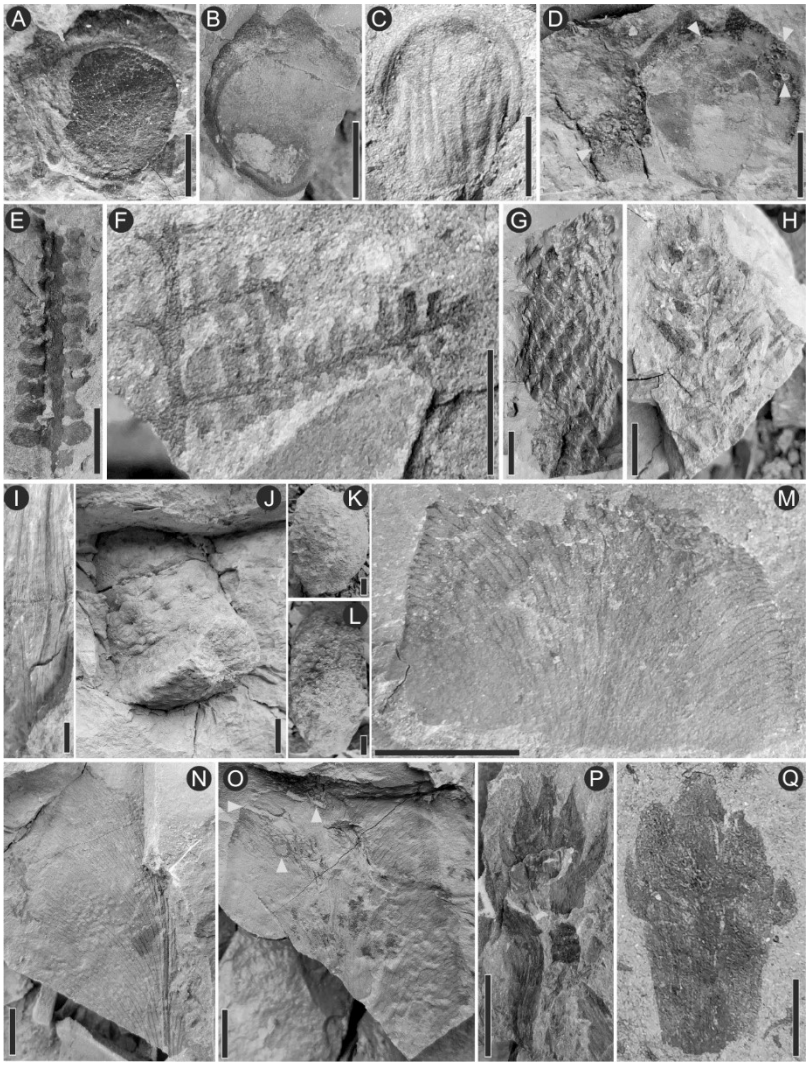

Figure 7

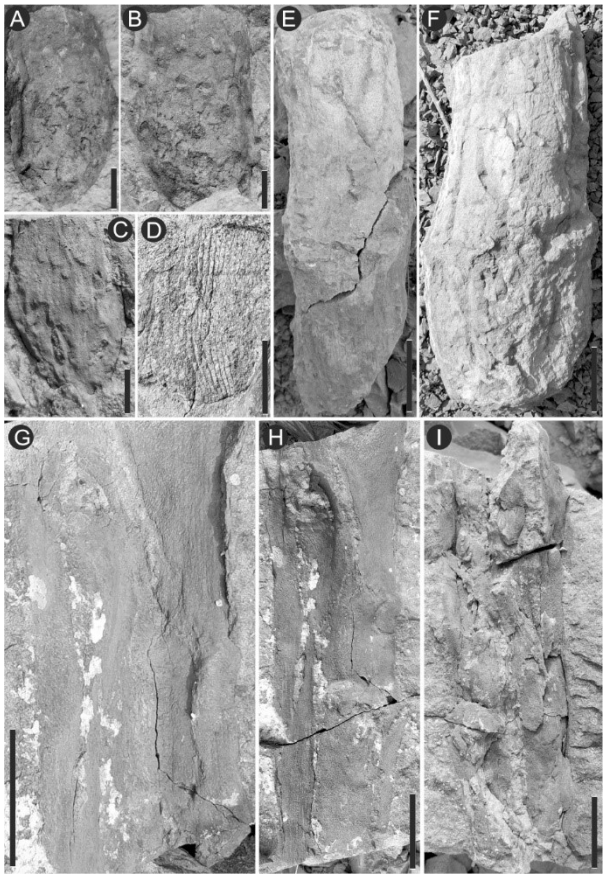

1231

1232 Figure 8

1233

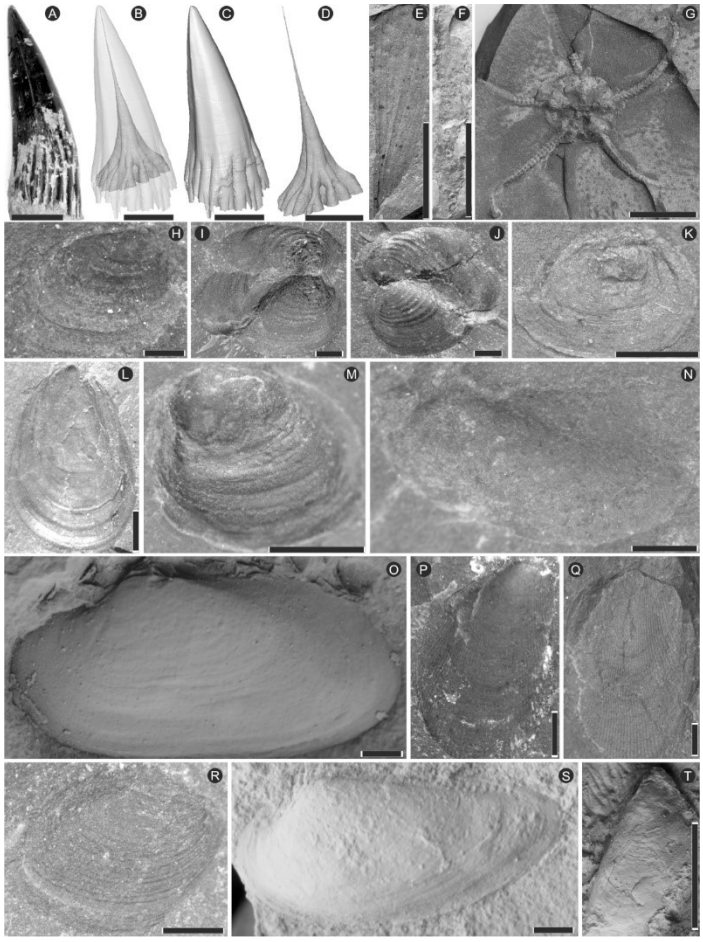

1234

1235 Figure 9

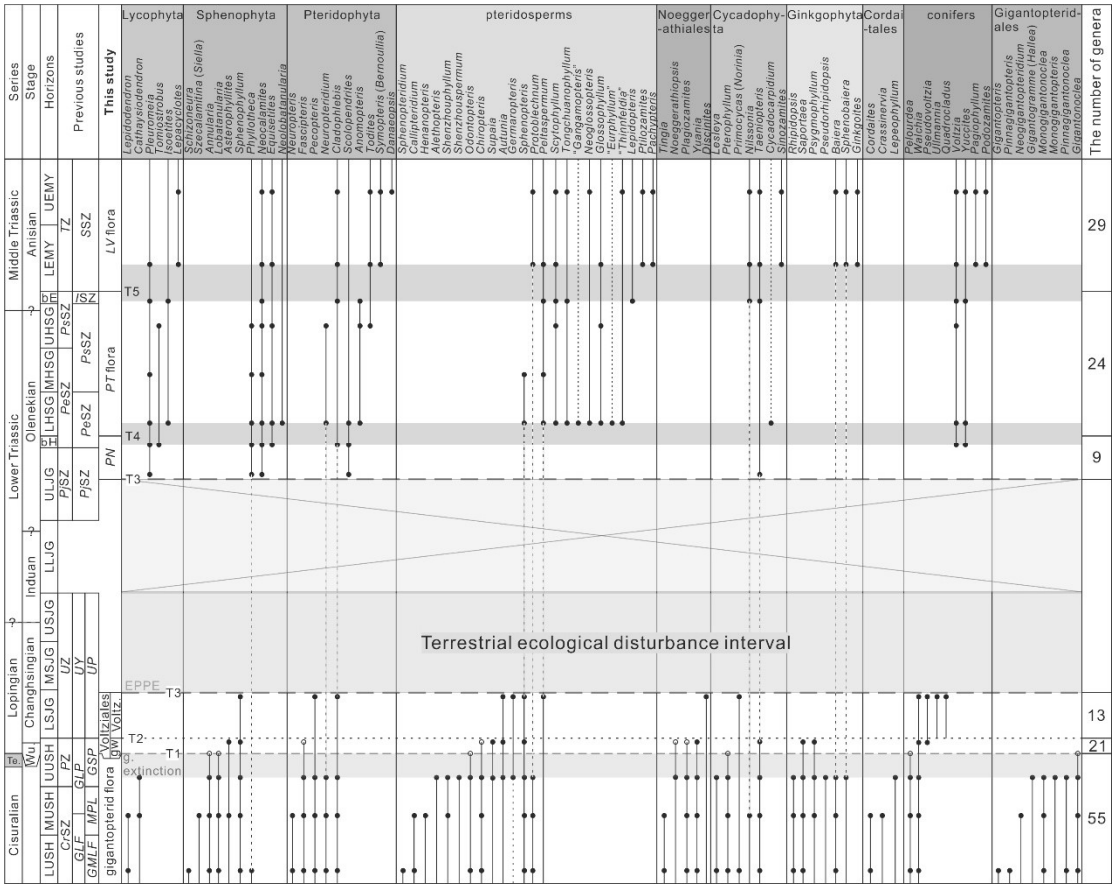

1236

1237 Figure 10

1238

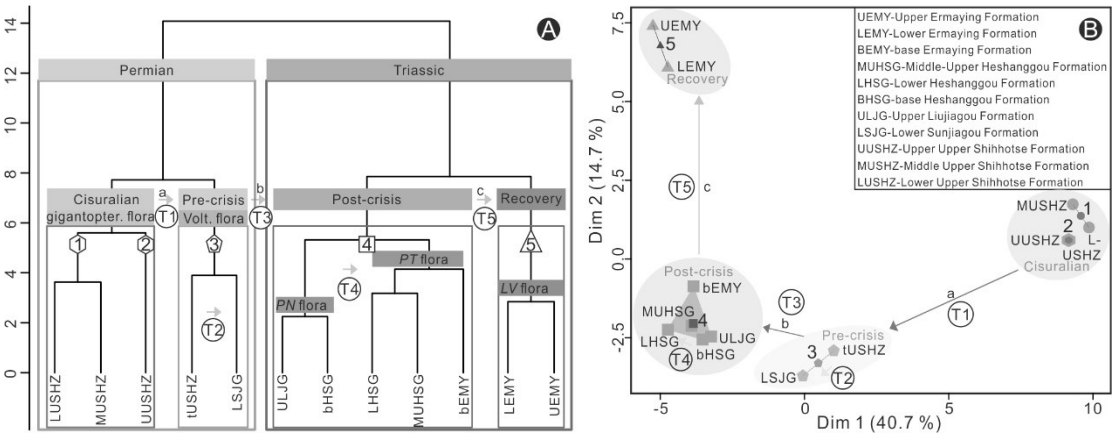

1239

1240 Figure 11

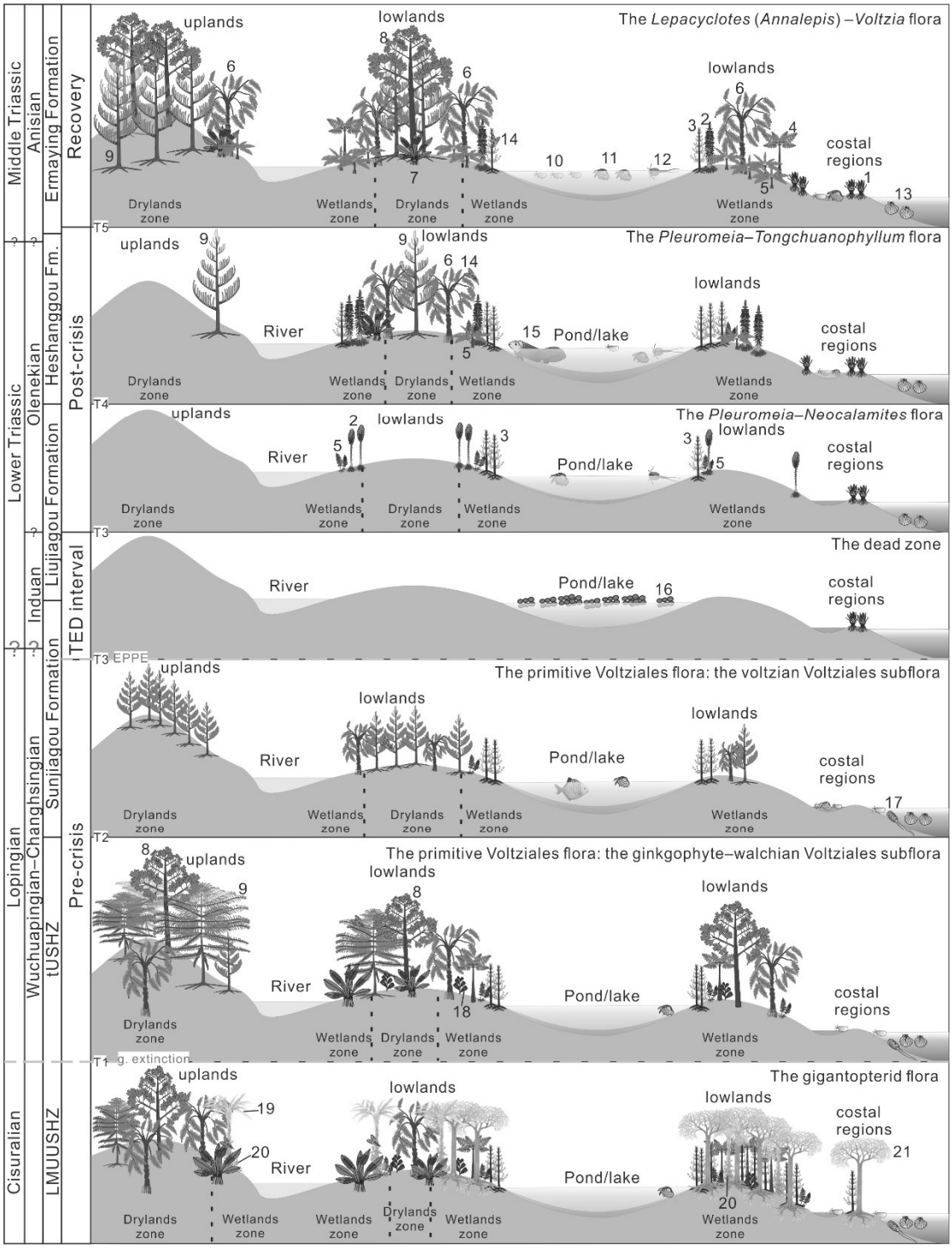

1241

1242 Figure 12

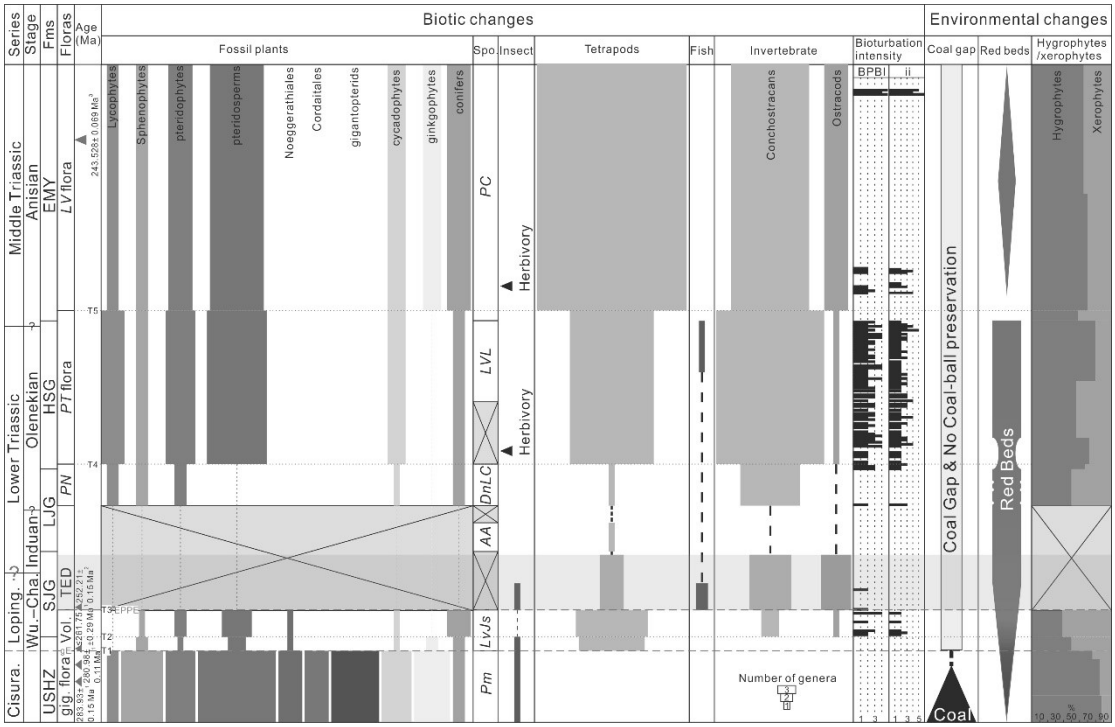

1243

1244 Figure 13

1245